DESIGN AND CHARACTERIZATION OF A MEMS MEMBRANE FOR A FIBER OPTIC MICROPHONE

A THESIS SUBMITTED TO
THE GRADUATE SCHOOL OF NATURAL AND APPLIED SCIENCES
OF
MIDDLE EAST TECHNICAL UNIVERSITY

BY

GÖKTUĞ CIHAN ÖZMEN

IN PARTIAL FULFILLMENT OF THE REQUIREMENTS
FOR
THE DEGREE OF MASTER OF SCIENCE
IN
ELECTRICAL AND ELECTRONICS ENGINEERING

MAY 2019

Approval of the thesis:

DESIGN AND CHARACTERIZATION OF A MEMS MEMBRANE FOR A FIBER OPTIC MICROPHONE

submitted by **GÖKTUĞ CIHAN ÖZMEN** in partial fulfillment of the requirements for the degree of **Master of Science in Electrical and Electronics Engineering Department, Middle East Technical University** by,

Prof. Dr. Halil Kalıpçılar
Dean, Graduate School of **Natural and Applied Sciences** ________________

Prof. Dr. Tolga Çiloğlu
Head of Department, **Electrical and Electronics Eng.** ________________

Prof. Dr. Barış Bayram
Supervisor, **Electrical and Electronics Eng., METU** ________________

Examining Committee Members:

Prof. Dr. Nevzat Güneri Gençer
Electrical and Electronics Eng., METU ________________

Prof. Dr. Barış Bayram
Electrical and Electronics Eng., METU ________________

Prof. Dr. Abdullah Atalar
Electrical and Electronics Eng., Bilkent University ________________

Assist. Prof. Dr. Serdar Kocaman
Electrical and Electronics Eng., METU ________________

Assist. Prof. Dr. Selçuk Yerci
Electrical and Electronics Eng., METU ________________

Date: 21.05.2019

I hereby declare that all information in this document has been obtained and presented in accordance with academic rules and ethical conduct. I also declare that, as required by these rules and conduct, I have fully cited and referenced all material and results that are not original to this work.

Name, Surname: Göktuğ Cihan Özmen

Signature:

ABSTRACT

DESIGN AND CHARACTERIZATION OF A MEMS MEMBRANE FOR A FIBER OPTIC MICROPHONE

Özmen, Göktuğ Cihan
Master of Science, Electrical and Electronics Engineering
Supervisor: Prof. Dr. Barış Bayram

May 2019, 74 pages

The most critical part of a fiber optic MEMS microphone is the sensing element. The sensing element, membrane, is designed such that the microphone operates in the desired range with desired sensitivity. In this thesis, a MEMS membrane is designed and characterized which is aimed to be used in a fiber optic microphone with responsivity to the audible frequency range. This membrane is electrically deflectable and it has symmetrically located air holes. The design is microfabricated through the commercially available multi-user multi-project service (POLYMUMPS, MEMSCAP Inc., France). The optical and electrical characterizations of the membrane are performed by impedance analyzer and laser vibrometer, respectively. Since the design is to be used in an optical interferometry based microphones, the surface of the membrane is coated by gold. The transient and steady state analysis of the membrane is utilized and both the overall and the spatial response of the membrane is obtained. The fundamental resonance of the membrane is 28 kHz. From laser vibrometer measurements under 100 mV peak-to-peak voltage and 1V DC bias conditions, the peak displacement is found to be 10 nm. The applied voltage is converted to the pressure and the sensitivity of the membrane is calculated to be 40 nm/Pa at 28 kHz. By spatial analysis of the design, symmetry is also verified. This thesis offers a new approach to the design of MEMS membrane for optical microphones.

Keywords: Fiber optic microphone, MEMS membrane, CMUT, POLYMUMPS

ÖZ

FİBER OPTİK MİKROFON İÇİN MEMS DİYAFRAM TASARIMI VE KARAKTERİZASYONU

Özmen, Göktuğ Cihan
Yüksek Lisans, Elektrik ve Elektronik Mühendisliği
Tez Danışmanı: Prof. Dr. Barış Bayram

Mayıs 2019, 74 sayfa

Bir fiber optik MEMS mikrofonunun en kritik kısmı, algılama elemanıdır. Algılama elemanı, yani diyafram, mikrofonun istenilen hassasiyette istenen aralıkta çalışacağı şekilde tasarlanmalıdır. Bu tezde, sesli frekans aralığına yanıt veren bir fiber optik mikrofonda kullanılması amaçlanan bir MEMS diyafram tasarlanmış ve karakterize edilmiştir. Bu diyafram elektriksel olarak bükülebilir olmakla birlikte, simetrik olarak yerleştirilmiş hava deliklerine sahiptir. Tasarım, ticari olarak temin edilebilen "multi-user multi project service" (POLYMUMPS, MEMSCAP Inc., Fransa) aracılığıyla mikro-üretilmiştir. Diyaframın optik ve elektriksel karakteristikleri sırasıyla empedans analizörü ve lazer vibrometre ile gerçekleştirilmiştir. Tasarım optik interferometri bazlı mikrofonlarda kullanılacağından, diyaframın yüzeyi altın kaplıdır. Membranın geçici ve denge durumu tepkileri analiz edilmiştir ve diyaframın hem genel hem de bölgesel tepkisi elde edilmiştir. Diyaframın temel rezonansı 28 kHz'dir. 100 mV tepeden tepeye gerilim ve 1V DC eğimleme gerilimi koşulları altında yapılan lazer vibrometre ölçümlerinden, en yüksek yer değiştirmenin 10 nm olduğu bulunmuştur. Uygulanan gerilim basınca dönüştürüldükten sonra diyaframın hassasiyeti 28 kHz'de 40 nm / Pa olarak hesaplanmıştır. Tasarımın bölgesel analizi yapılarak simetri de doğrulanmıştır. Bu tez, optik mikrofonlar için MEMS membranının tasarımında yeni bir yaklaşım sunmaktadır.

Anahtar Kelimeler: Fiber optik mikrofon, MEMS diyafram, CMUT, POLYMUMPS

To my family, and the love and light of my life Güliz

ACKNOWLEDGEMENTS

This thesis is supported by The Scientific and Technological Research Council of Turkey (TÜBİTAK) (PI: Prof. Dr. Barış Bayram, project no: **215E090**) and Middle East Technical University (BAP) (PI: Prof. Dr. Barış Bayram, project no: **BAP-03-01-2018-004**).

During the procession of this study, the author acknowledges the financial support of TUBITAK BIDEB 2210-A 2017-1 Scholarship.

First, I would like to express my kind respect and thank Prof. Dr. Barış Bayram for his advanced supervision, enlightening guidance and support. He has not only supported me academically, but also prepared me to a lifelong journey. It would not be possible to improve myself, produce good outcomes from my research and achieve my goals without his existence, supervision and support.

I would like to thank Prof. Dr. Nevzat Güneri Gençer, Assist. Prof. Dr. Serdar Kocaman, Assist. Prof. Dr. Selçuk Yerci and Prof. Dr. Abdullah Atalar for being on my thesis committee.

I would like to thank Assoc. Prof. Asaf Behzat Şahin for his technical support.

I want to give my special thanks to Mr. Ekin Muharrem Karaca for being my colleague who was always there to help and support me in our last three years.

I would like to thank Mr. Yiğit Özer for his technical comments, and valuable friendship.

I would like to thank the members of ULTRAMEMS Research Group, Ms. Asude Aydin, Ms. Eda Begüm Berberoğlu, Ms. Cansu Demirkıran, Ms. İrem Kozakçı, Mr. Mert Karamancı, Ms. Tansu Demirci, Ms. Zeynep Ayhan, Ms. İris Çelebi, Mr. İlker

Oğuz, Ms. Doğa Buse Çavdır and especially to Mr. Anıl Bozyiğit, Mr. Murat Arslan and Mr. Berkay Karacaer for their technical support and useful discussions.

I would like to thank METU TTO Director Ms. İdil Buse Kök and staff Mr. Yusuf Dudu for their helpful approach during the patent disclosure of our study.

I would like to thank METU BAP Coordinator Assoc. Prof. Dr. Hüsnü Dal and administrative staff Ms. Azize Cabadağ Şiret, Head of METU Foreign Purchasing Directorate Mr. Mikail Yılmaz and administrative staff Mr. Mustafa Altınışık, Mr. Hayrullah Başoğlu, and METU Department of Strategy Development Director Mr. Ali Seyhan and staff Mr. Volkan Macit for their support on administrative procedures.

Finally, I want to express my deep appreciation to my love Güliz, and my family, for their endless support.

TABLE OF CONTENTS

LIST OF TABLES

TABLES

LIST OF FIGURES

FIGURES

CHAPTER 1

INTRODUCTION

Microelectromechanical systems (MEMS) are the integrated micro devices or systems relating electrical and mechanical components developed by using Integrated Circuits (IC) compatible batch-processing techniques and range in size from micrometers to millimeters. They are widely used as sensors, control elements or actuators on micro scale to generate macro scale effects.

MEMS technology is known to exist for at least five decades, so far. The technology has involved in physics, chemistry and biology as the origin of sensors. Today, very small MEMS devices are being fabricated such that they cannot be seen by human eye. Small size of these devices make them suitable for small area and low power applications.

MEMS is, today, a well-established research area accepted by the researchers all over the world. In this area, mechanical elements like cantilevers or membranes had been developed and manufactured at a scale closer to microelectronics circuits. MEMS are small integrated devices or systems that brings together electrical and mechanical components [1].

As MEMS technology develops in the last decades, electret condenser microphones have been replaced more and more by silicon MEMS microphones, because of their durable and reliable performance characteristics at high temperature or high humidity [2]. In applications such as mobile phone communications, silicon MEMS microphones become state of the art. With the advances in this technology, researchers achieved high signal to noise ratio (SNR), high sensitivity and small size microphones [3].

In commercially available MEMS microphones, detection is utilized through electrical measurements such as current/voltage measurements or capacitive measurements. With the current technology, these electrical measurements are highly vulnerable to the electrical noise originated from the system or the environment. Furthermore, these electrical measurements do not yield true results under extreme conditions such as high temperature or high pressure. Fiber optical sensors are used in a wide range of applications for temperature, vibration, pressure, index of refraction sensing. By combining MEMS technology with the fiber optic sensing with extrinsic Fabry-Perot interferometry, it becomes possible to make the detection of high frequency ultrasonic signals with high precision [4].

Today, in some special applications, such as measurement in harsh environments, fiber optic microphones are preferred over condenser microphones. The conventional condenser microphone is a high impedance device due to the necessity of a high input impedance preamplifier for further signal processing [4,5]. The additional high impedance preamplifier seems to be an additional imposition in the design. This results in the reduction of performance of the microphone even with sophisticated electronic designs. In addition, there is a limitation on the distance between the microphone and the receiver electronics due to the cable capacitances. This situation limits the application of the microphone in a confined space.

The fiber optic MEMS microphone has very high resistance to electromagnetic interference since all of the electronic components that is used in the design are kept out of the sensor probe [4]. One of the major advantages that MEMS technology offers is the flexibility to achieve the desired response range, bandwidth, and sensitivity by basically adjusting the size of the membrane [5].

There are two methods used in fiber optic MEMS microphones: phase and intensity modulation. It was shown that phase modulation technique gives better performance considering the measurement range and durability [5,6]. These reasons suggest the necessity of finding a new way of designing a MEMS microphone for audible frequency range. It was shown that utilization of light as the way of detect sound waves gives much better performance than the microphones which senses the sound electrically [7].

The unique advantages of optical sensing technique, such as immunity to electromagnetic interferences, stability, repeatability, durability against harsh environments, high sensitivity, high resolution and fast response, makes it vital for industrial non-destructive techniques, vibration and design and testing of microstructures [6]. The fiber optic microphone can enable innovative applications in a variety of applications due to the wide dynamic range, high sensitivity and flat frequency response over large bandwidth [4].

Extrinsic Fabry-Perot interferometer based pressure sensors become popular in the last decades and substantial research has been carried out on it. It was shown that diaphragm-based extrinsic Fabry-Perot interferometer sensors are commonly used for low pressure and acoustic wave detection with success [8].

The most important part of the high fidelity Fabry-Perot interferometer based pressure sensor is its MEMS membrane. The laser light propagating through the fiber optic cable leaves the fiber, hits the membrane and reflects back to the fiber end. Between the fiber end and the membrane, a Fabry-Perot cavity is obtained. By this cavity, even small displacements in the membrane can be detected by analyzing the interference fringes. Compared to intensity modulation technique, phase modulation technique has been proven to be feasible by experimental measurements [7].

The electrical impedance of the membrane in the air can be arranged by changing the size of the membrane. The fiber optic MEMS microphone can also be extended to measure vibration and acceleration due to its immunity to changes in temperature, pressure and vibration. Since the design is simple and the operation of the device is easy, it can be used in a variety of applications [7]. In addition to the audible wave detection, fiber optic idea can also be used to measure pressure. It is shown that linear pressure sensitivity between 0 kPa and 600 kPa is achieved in the temperature range of 20 ºC - 300 ºC with fiber optic based pressure sensors.

With the research that is ongoing on fiber optic MEMS microphone, different membrane materials, such as graphene oxide and Parylene-C, are proposed to be used in the fiber optic microphones [9]. Parylene-C gives strong response in the order of 2000nm/Pa at 20 Hz. Since Parylene-C is a bio-compatible, these acoustic sensors are suggested to be used in biomedical applications [9]. Nowadays, there is a huge research that is carried out on graphene oxide, and its reliable production became possible with any desired thickness. These developments led the utilization of graphene oxide as the membrane material and these sensors give flat response in 100 Hz – 20 kHz range [10].

In addition to the motivation of finding new materials for the membrane of the fiber optic microphones, new membrane designs are also investigated with standard silicon process materials. It is shown that corrugated silver membranes can be used for optical fiber microphones. The corrugations on the membrane was shown to improve the performance of the microphone, the responsivity of this new design is in the order of 50nm/Pa in the range of 63 Hz – 1 kHz [11]. Recently, it is also suggested to microfabricate an annular corrugated MEMS membrane. The new design is able to sense the minimum pressure level of 3 $\mu Pa/Hz^{1/2}$ at 1 kHz.

The Contribution of the Thesis

- A novel membrane is designed and characterized for fiber optic MEMS microphone application.
- The membrane is sensitive to the audible frequency range (20 Hz – 20 kHz).
- The membrane design is compatible with the optical sensing for detection of the membrane displacement. The membrane is coated by optically reflective gold layer.
- The mature and well-known microfabrication process, POLYMUMPS (MEMSCAP Inc., France) is used to obtain a reliable and reproducible design.

- A membrane with air holes is designed. The placement of the holes is studied and optimized to achieve high fill factor and to obey the design rules of POLYMUMPS.
- The operation of the new MEMS membrane is verified through extensive steady state and transient analysis with different characterization setups.
- The response of the membrane under different excitations is investigated and the performance of the device is verified.
- The resonance frequency of 28 kHz is achieved by 1000 μm – diameter circular membrane.
- The sensitivity of the membrane is found to be 40 nm/Pa at 28 kHz.
- Two other resonance frequencies are observed at 51 kHz and 109 kHz.
- The membrane is highly symmetric and the center of the membrane gives high response at three of the resonances.
- The membrane is found to be compatible with optical microphones with its optically reflective gold coated membrane, its fundamental mode at 28 kHz and its high symmetry.

CHAPTER 2

DESIGN OF THE MEMS MEMBRANE

2.1. Selection of the Microfabrication Process

The fiber optic MEMS microphone consists of two fundamental parts, the sensing element of the microphone which is the membrane and the optical detection part. The mechanical and electrical properties of the sensing element of the fiber optic MEMS microphone are highly important. For high quality detection and long term usage, the membrane of the microphone should be reproducible, durable and stable. Lack of these properties may result in faulty detection of the sound even with a high quality optical detection system.

These concerns are considered in the microfabrication process. There are different foundries offering multi-user multi-processes (MUMPS) that are commercially available. Each of these processes offer different flexibilities and advantages. The compatibility of each process with designing the membrane of the fiber optic MEMS microphone is carefully analyzed and the POLYMUMPS process (MEMSCAP Inc., France) is selected. This decision was made based on its ability to offer non-limiting MEMS designs, and the positive results researchers have obtained and recorded in the literature whilst using POLYMUMPS process for device microfabrication [14-19].

2.2. POLYMUMPS Process

POLYMUMPS is a three-layer polysilicon surface micromachining process. The basis of this process comes from the studies in Berkeley Sensor and Actuator Center (BSAC) at California University between 1980 and 1990. After finalizing several different microfabrication processes and analyzing the feedback from the users, the process is developed further and the microfabrication steps are fine-tuned.

With these development, high-tech device fabrication became possible and now, more advanced devices can be fabricated on a single chip. Today, this process is commonly utilized in universities and companies all over the world.

2.2.1. POLYMUMPS Process Flow

In POLYMUMPS process, <100> crystal direction, n-type silicon wafers with 1-2 Ω-cm resistivity and 150 mm diameter are used. First, the surface of the wafer is heavily doped by phosphorus (P) atoms. At this point, phosphorus doped silicate glass (PSG) is used as the source of the doping. The purpose of this layer is to avoid electrical short circuit between different design on the wafer and to stop the static electric flow. The PSG layer is removed after the doping is utilized through diffusion. Then, 600 nm-thick silicon nitride layer with low internal stress is deposited on the wafer through low pressure chemical vapor deposition (LPCVD) process [13].

After the silicon nitride layer is deposited, the first polysilicon layer, POLY0, is deposited through LPCVD process. The thickness of POLY0 layer is 500nm. This layer is shaped by using POLY0 and HOLE0 masks. Then, the first oxide layer is deposited on the wafer which is 2 μm-thick. This oxide layer will be removed at the end of the process and other polysilicon layers on top of this oxide layer will be able to move freely in the air. The first oxide layer is also shaped by ANCHOR1 and DIMPLE masks. ANCHOR1 mask indicate at which points second polysilicon layer, POLY1, will be grown directly on top of POLY0. At these indicated areas in the mask, first oxide layer will be totally removed. DIMPLE mask is optional to use and it removes 750 nm of oxide at the indicated points. The small holes in the first oxide layer propagates till the end of the process through the surface. The holes will be filled by either the second or third polysilicon layers, POLY1 or POLY2. Since the oxide layers will be removed by wet etch followed by dry etch, moving designs, such as a membrane, can be stick to the surface by adhesion force of the liquid. Once the design is stick, it may no longer be removed and the design will be useless. These small dimples will decrease the surface of contact between the moving element and the wafer which will significantly decrease the chance of adhesion problem [13].

After the first oxide layer is shaped, the second polysilicon layer, POLY1, is grown on the wafer. The thickness of this layer is 2 μm and it is called as the first mechanical polysilicon layer. The company suggests not to use POLY0 layer for mechanical purposes, but to use POLY1 and POLY2 layers for mechanical purposes. On top of POLY1, a thin PSG layer is deposited and this structure is annealed at 1050 ^{o}C for an hour. The purpose of this process is to dope the polysilicon layer with P atoms through diffusion to make it an n-type polysilicon. This annealing process also removed the internal mechanic stress in POLY1. The second polysilicon layer, POLY1, is shaped by POLY1 and HOLE1 masks. After shaping POLY1, the second oxide layer is deposited on the wafer. The second oxide layer is shaped by POLY1-POLY2-VIA and ANCHOR2 masks. POLY1-POLY2-VIA mask indicates the regions where POLY2 will directly be grown on POLY1. ANCHOR2 mask indicated the regions there POLY2 will directly be grown on POLY0. ANCHOR2 mask should be utilized wisely since improper ANCHOR2 design should result in faulty results. For example, in order to grow POLY2 directly on POLY0, there should not be any POLY1 layer between them. If the designer forgets that POLY1 layer exists under some region of the second oxide and designs ANCHOR2 mask in a way that ANCHOR2 mask regions and POLY1 regions overlap, then POLY2 cannot be directly grown on POLY0 [13].

After the second oxide layer is shaped, the third polysilicon layer, POLY2, is grown on the wafer. POLY2 is the second mechanical polysilicon layer. POLY2 layer is 1.5 μm-thick and a thin PSG layer is deposited on it. The structure is annealed at 1050 ^{o}C for an hour. The purpose of annealing is to dope POLY2 by P atoms to make it n-type and to remove the mechanical stress in it. POLY2 layer is shaped by POLY2 and HOLE2 layers [13].

After all polysilicon and oxide layers are shaped, metal layer is deposited on the wafer and shaped by liftoff process using METAL and HOLEMETAL masks. This metal layer can be used for electrical contacts as well as for creating optically reflective surfaces.

Finally, the design is wet etched to remove the oxide layers. During wet etch, the dissolved oxide in one design may propagate through another design and stick to it. This will cause a problem. For that purpose, first, to avoid any damage, different designs on a single wafer are separated by dicing. Then, the designs are put into 49 % HF solution at room temperature and they are left for 1.5-2 hours. After wet etch, the chips are put in distilled water for a few minutes and then they are put in alcohol again for a few minutes. Finally, the chips are annealed in an oven at 100 °C for 10 minutes. In some designs, designer may want to etch the oxide further through supercritical CO_2 dry etch. In such cases, the chips will be put in CO_2 gas for the dry etch of the oxide layers.

After the removal of oxide layers, the fabrication is finalized and the chips become ready for delivery to the designer.

2.2.2. POLYMUMPS Design Rules

The purpose of the design rules is to guide the designer toward error-free designs. These design rules are developed by the experience of company employers and the feedback from the designers. The design rules are created by the decision on each process step rule considering the limitations of the process. The main aim of design rules is to obtain stable processes. Fundamentally, the minimum feature size comes from the limitations of the microfabrication devices such as photolithography device resolution [13].

There are two types of design rules for POLYMUMPS process: mandatory and advisory design rules. The violation of mandatory design rules may result in undesired and unpredictable damages on the designs. In fact, MEMSCAP has the right to remove a design which violates mandatory design rules. On the other hand, advisory design rules should be considered as the advice of the company employers to achieve the free-of-fault microfabrication of the design [13].

Design rules, in general, indicate the distance between different layers and the considerations under the situations of overlapping of different layers. Nevertheless, design rules are the extreme limits. In other words, there should be some safety margin beyond the design rules. The layers in the POLYMUMPS process, their thicknesses and the corresponding masks for each layer are given in Table 2.1 [13].

Table 2.1. *POLYMUMPS process layers, their thicknesses and corresponding microfabrication masks [13].*

Layer Material	*Layer Thickness (μm)*	*Microfabrication Masks*
Silicon Nitride	0.6	--
POLY0	0.5	POLY0 (HOLE0)
First Oxide	2.0	DIMPLE ANCHOR1
POLY1	2.0	POLY1 (HOLE1)
Second Oxide	0.75	POLY1-POLY2-VIA ANCHOR2
POLY2	1.5	POLY2 (HOLE2)
Metal	0.5	METAL (HOLEM)

In Table 2.1, it is given that each polysilicon layer has two masks. In fact, this is the flexibility that MEMSCAP gives to the designer. These masks will be merged before microfabrication, but since etch holes are required during oxide wet etch, hole design is mandatory. Designer may confuse with etch holes and actual shaping of each layer on the same mask. To avoid this, etch holes can be drawn on HOLE masks while other shaping structures can be drawn on POLY and METAL masks.

2.2.2.1. Mandatory Design Rules

In the process, the polysilicon layer masks are defined as light while the oxide layer masks are defined as dark. While designing light masks, the regions that the designer wants not to remove should be drawn. On the other hand, while designing dark masks, the regions that the designer wants to remove should be drawn. The design masks, their light/dark properties and their purposes are given in Table 2.2 [13].

Table 2.2. *POLYMUMPS process masks and their properties [13].*

Mask Name	*Mask Type*	*Mask Purpose*
POLY0	Light	Shaping POLY0
ANCHOR1	Dark	Creating contact holes between POLY1 and POLY0
DIMPLE	Dark	Creating tiny holes for POLY1
POLY1	Light	Shaping POLY1
POLY1-POLY2-VIA	Dark	Creating contact holes between POLY2 and POLY1
ANCHOR2	Dark	Creating contact holes between POLY2 and POLY0
POLY2	Light	Shaping POLY2
METAL	Light	Shaping METAL
HOLE0	Dark	Crating holes for POLY0
HOLE1	Dark	Crating holes for POLY1
HOLE2	Dark	Crating holes for POLY2
HOLEM	Dark	Crating holes for METAL

The purposes and properties of microfabrication masks should guide the designer for proper designs. In addition to the properties, the mandatory design rules for microfabrication masks are given in Table 2.3. These rules are the minimum required dimensions for each case. For reproducible designs, safety margins should be applied to these limits.

Table 2.3. *POLYMUMPS mandatory design rules for process masks [13].*

Rule	*Minimum Value (µm)*
Distance between POLY0 and ANCHOR1	4.0
POLY0 encloses ANCHOR1	4.0
POLY0 encloses POLY1	4.0
POLY0 encloses POLY2	5.0
POLY0 encloses ANCHOR2	5.0
POLY1 encloses ANCHOR1	4.0
POLY1 encloses POLY1-POLY2-VIA	4.0
POLY1 encloses POLY2	4.0
Distance between POLY1 and ANCHOR2	4.0
Distance between POLY1 etch holes	**MAX** 30.0
POLY2 encloses ANCHOR2	5.0
POLY2 encloses POLY1-POLY2-VIA	4.0
POLY2 overlaps POLY1	5.0
In POLY2 overlaps POLY1 case, distance between POLY2 and POLY1 edge	4.0
POLY2 encloses METAL	3.0
Distance between POLY2 and POLY1	3.0
HOLE2 encloses HOLE1	2.0
HOLEM encloses HOLE2	2.0
Distance between POLY2 etch holes	**MAX** 30.0

2.2.2.2. Advisory Design Rules

In addition to the mandatory design rules declared by MEMSCAP, there are some advisory design rules based on previous experiences with POLYMUMPS. These rules are not mandatory, but MEMSCAP declares that the designs that do not take into account them will be on the designer's responsibility. Therefore, advisory design rules are so important that they should also be considered during the design of microfabrication masks [13].

2.2.2.2.1. Hole Usage and Its Density

By utilizing ANCHOR1, ANCHOR2 and POLY1-POLY2-VIA masks, holes between different layers can be obtained. It is important to note that these holes are not etch holes. According to MEMSCAP, beginner level designers sometimes use oxide holes without any need and then they do not fill these holes with corresponding polysilicon layers. This situation would create two problems. First, the polysilicon layers in these holes may be etched in stair shapes, which may lead to unpredictable consequences. Secondly and most importantly, the polysilicon under these holes may be unintentionally etched in the later process steps. As a result, the useful polysilicon layers may be damaged [13].

2.2.2.2.2. Improper Dimensions of ANCHOR and VIA holes

Improper dimensions of oxide holes may result in the deviation of the positions of these holes. Therefore, without any important purpose, the size of the polysilicon layer should be larger than the size of the hole. This situation is applicable to both POLY1 and POLY2 layers [13].

2.2.2.2.3. Improper PAD Design

There would be problems in the case that the electrical pads are designed improperly without considering enclosure limits between different layers. Some users previously reported that placement of electrical pads near unintentionally etched silicon nitride regions results in problems. The reason is the electrical short circuit between the silicon wafer and the electrical pads. To avoid such problems, designers should ask MEMSCAP for proper electrical pad design and use it as it is. MEMSCAP does not charge for this and shares the pad design file [13].

2.2.2.2.4. Utilization of Metal Layer

In POLYMUMPS process, it is most suitable to grow metal layer on top of POLY2. The reason comes from the oxygen free surface of POLY2. Some beginner level designers may grow metal directly on the oxide layers and after the oxide etch, there occur serious problems in the design such as electrical short circuit [13].

In addition to that, for proper growth of metal on POLY2, this chromium layer is used between these layers. This chromium layer improves the ability of metal to stick to POLY2. This coating process is utilized through liftoff. Sometimes, during liftoff, some metal regions may be lifted off unintentionally. The reason comes from photolithography errors. According to MEMSCAP, the surface that metal can stick to polysilicon layer through thin chromium layer is the POLY2 surface [13].

2.2.3. POLYMUMPS Process Thin Film Parameters

In POLYMUMPS process, there are one silicon nitride layer, three polysilicon layers, two oxide layers and one metal layer. MEMSCAP gives properties of each layer according to the measurement taken during and after the microfabrication process. This data is taken for each microfabrication run and mean and extreme values are given to the designer. The properties of layers are given is Table 2.4. [13]

Table 2.4. *POLYMUMPS process layer properties [13].*

Layer (Film)	*Thickness (A^o)*			*Residual Stress (MPa)*			*Resistance (Ω/sq)*		
	Min.	Typ.	Max.	Min.	Typ.	Max.	Min.	Typ.	Max.
Silicon Nitride	5300	6000	6700	0	90	180		N/A	
POLY0	4700	5000	5300	0	-25	-50	15	30	45
First Oxide	17500	20000	22500		N/A			N/A	
POLY1	18500	20000	21500	0	-10	-20	1	10	20
Second Oxide	6700	7500	8300		N/A			N/A	
POLY2	14000	15000	16000	0	-10	-20	10	20	30
Metal	4600	5200	5800	0	50	100	0.05	0.06	0.07

2.3. Theoretical Design of the Membrane

The membrane of the fiber optic MEMS microphone is the fundamental sensing element. The characteristics of the system is mainly restricted by the characteristics of the membrane. There are different membrane designs and sensing approaches exist in the literature. In table 2.5, different MEMS microphones with their properties is represented. There are examples of capacitive, piezoresistive and piezoelectric microphones.

Table 2.5. MEMS microphones in the literature and their properties.

Microphones	Transducer Type	Sensor Dimensions	Sensitivity	Dynamic Range	Bandwidth
1- Sheplak et.al. 1998 [20,21]	Piezoresistive	105µm x 0.15µm	2.24 µV/Pa/V	92 dB – 155 dB	200 Hz – 6 kHz
2- Huang et.al. 2002 [22]	Piezoresistive	710µm x 0.38µm	1.1 mv/Pa/V	53 dB – 174 dB	100 Hz – 10 kHz
3- Scheeper et.al. 2003 [23]	Capacitive	1950µm x 0.5µm	22.4 mV/Pa	23 dB – 141 dB	251 Hz – 20 kHz

4- Martin et.al. 2007 [24,25]	Capacitive	230µm x 2.25µm	390 mV/Pa	41 dB – 164 dB	300 Hz – 20 kHz
5- Martin et.al. 2008 [26]	Capacitive	230µm x 2.25µm	166 µV/Pa	22.7 dB – 164 dB	300 Hz – 20 kHz
6- Chan et.al. 2010 [27]	Capacitive	--	12.63 mV/Pa	--	500 Hz – 20 kHz
7- Yang et.al. 2010 [28]	Capacitive	450µm diameter	14.45 mV/Pa	--	--
8- Chao et.al. 2013[29]	Capacitive	--	1.7 mV/Pa	--	100 Hz – 10 kHz
9- Franz et.al. 1988 [30]	Piezoelectric (AlN)	0.72mm^2 x 1µm	25 µV/Pa	68 dB - --	-- - 45 kHz
10- Horowitz et.al. 2007 [31]	Piezoelectric (PZT)	900µm x 3.0µm	1.66 µV/Pa	35.7 dB – 169 dB	100 Hz – 6.7 kHz
11- Litrell et.al. 2010 [32]	Piezoelectric (AlN)	0.62mm^2 x 2.3µm	1.82 mV/Pa	37 dB – 128 dB	50 Hz – 80 kHz
12- Grosh et.al. 2013 [33]	Piezoelectric (AlN)	--	0.71 mV/Pa	--	--
13- Lee et.al. 2008 [34]	Piezoelectric	--	8.1 mV/Pa	--	--

Since POLYMUMPS will be used in microfabrication, piezoresistive and piezoelectric designs are not analyzed in detail. However, capacitive MEMS microphones' membranes are very similar to the membrane of a fiber optic MEMS microphone. Basically, two plates, one being stable and one moving, are present in both of them. Therefore, membrane designs of capacitive microphones are valuable and should be considered.

The most important parameters of capacitive MEMS microphones in Table 2.5 are the bandwidth and the dimensions. In order to sense sound in audible frequency range (20Hz – 20kHz), the membrane should be sensitive in this range [35]. Another concern is the phase response of the membrane. To obtain the sound properly, the frequencies should feel almost constant phase, otherwise the sound can be disturbed. A membrane with resonance frequency of 25-30 kHz can sense the audible frequencies and give almost constant phase response to them.

Considering this resonance frequency and the audible frequency range, the microphones 4,5 and 6 in Table 2.5 seem to be utmost interest. The number 4 microphone has air holes in the design. This design is valuable in a way that POLYMUMPS process requires etch holes and they will result in a membrane with holes. The membrane design in the number 4 microphone is as shown in Figure 2.1 [24].

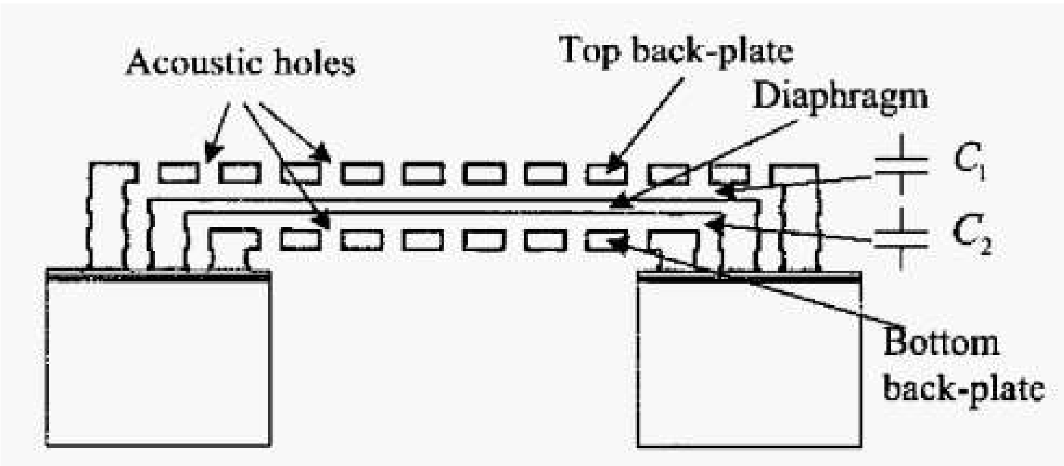

Figure 2.1. Capacitive membrane with holes [24].

The acoustic holes in Figure 2.1 are very similar to the holes required by POLYMUMPS; they are periodic and placed all over the membrane. In this design, the MEMS process, so called 'SUMMIT V', is used. This process includes sacrificial oxide layers as in POLYMUMPS. In 'SUMMIT V', etch holes are required such that the sacrificial oxide layers can be etched after the process. In this article, it was shown that the holes improve the acoustic performance of the membrane. The obtained sensitivity and phase response data for this microphone is as shown in Figure 2.2.

In Figure 2.2, it is shown that the microphone operates in 300 Hz – 20 kHz frequency band and the phase that the system introduces to the input signals is smaller than 20° for the frequency range of 1 kHz – 20 kHz). The membrane in this microphone is circular and its diameter is 460μm. There is no specific information on the resonance frequency of the membrane, but it can be inferred from the phase response that there are several resonance frequencies in the frequency range of interest. Therefore, the results of this article are highly important for the membrane design for audible frequency detection in fiber optic MEMS microphone.

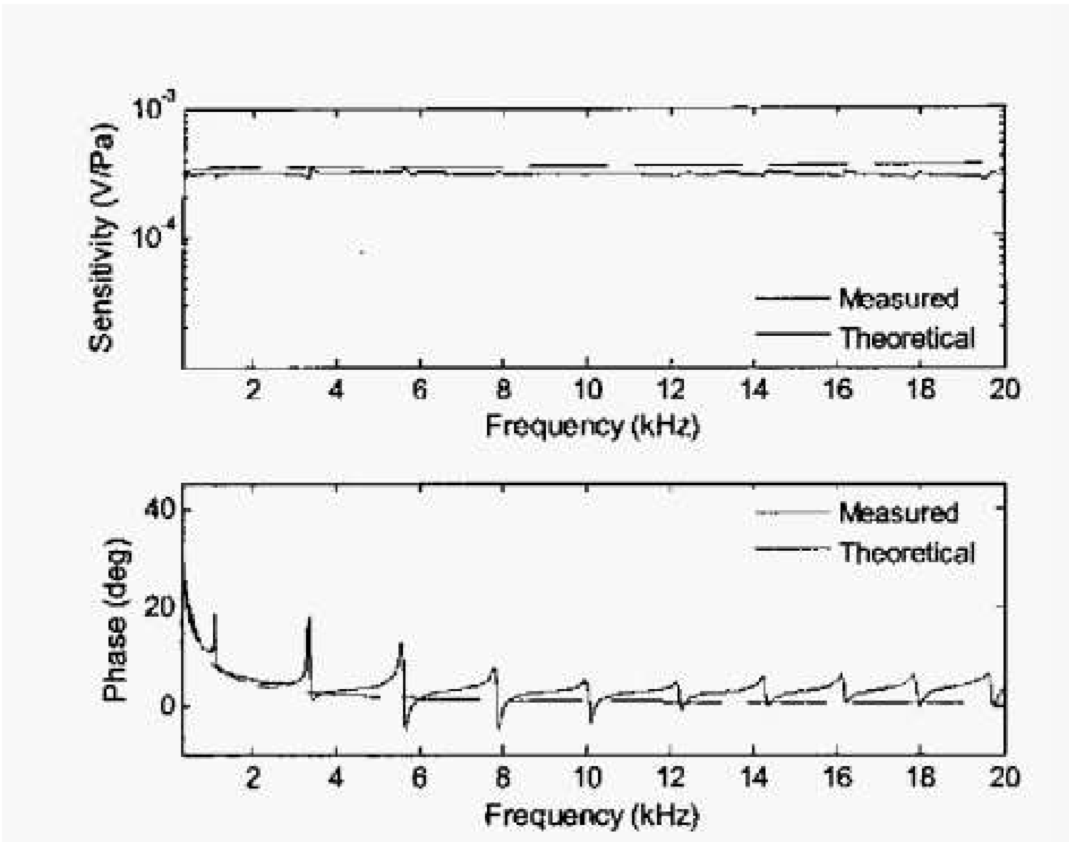

Figure 2.2. The test results of capacitive microphone [24].

The number 5 microphone is also fabricated with 'SUMMIT V' process. The membrane of this microphone is as shown in Figure 2.3 [25].

In this design, it is clearly shown that there are three layers of polysilicon, one as the membrane and the other two as the carrying material of the membrane. Air holes are also shown in Figure 2.3. The membrane in this design has the diameter of 460μm and the resonance frequency of 174 kHz. In addition, this membrane gives response to the frequency range of 300 Hz – 20 kHz. The bandwidth and the physical structure of the membrane overlap with the requirements of the membrane of a fiber optic MEMS microphone.

From the literature, it is clear that the physical structure of the membrane is highly important. Nevertheless, since the reviewed articles cover capacitive sensing, the resonance frequencies of these membranes are much higher than the audible range. For fiber optic MEMS microphone, on the other hand, high responsivity in the audible frequency range is desired and there should be no phase reversal in this range. In order to achieve both of them at the same time, the first resonance frequency should be around 25 - 30 kHz.

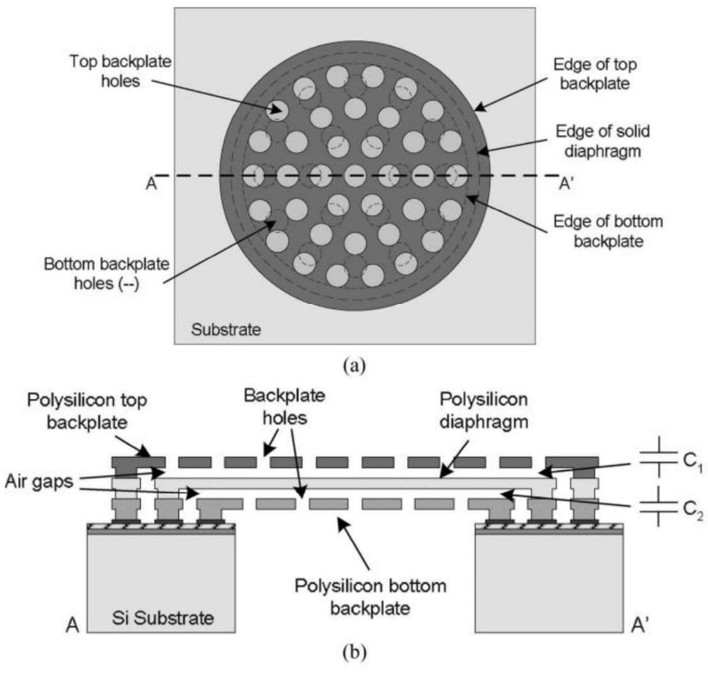

Figure 2.3. (a) Top view, and (b) cross-sectional view of the membrane of the capacitive microphone [25].

2.3.1. The Diameter of the Membrane

The parameters governing the first resonance frequency of a membrane are its material properties and dimensions. For a circular membrane, this relation is given by

$$f = \frac{10.21}{2\pi a^2}\sqrt{\frac{Eh^2}{12\rho(1-\mu^2)}} \quad (1)$$

The meaning of the parameters in (1) and their values obtained from MEMSCAP are given in Table 2.6 [13]. Since POLYMUMPS process will be used for fabrication of the membrane, its parameters are used.

The first resonance frequency of a circular membrane for different radius values are as shown in Figure 2.4.

Table 2.6. *Parameters of first resonance frequency of a circular membrane and their values for POLYMUMPS process [13].*

Parameter	*Value*
E (Young's modulus of polysilicon)	168 GPa
μ (Poisson's ratio of polysilicon)	0.22
ρ (Mass density of polysilicon)	2.3 g/cm^3
h (Thickness of polysilicon membrane)	1.5239 μm
a (Radius of polysilicon membrane)	Variable in μm

It is clear from (1) and Figure 2.4 that as the radius of the membrane increases, the first resonance frequency decreases. For the fiber optic MEMS microphone, it is aimed to obtain a membrane with first resonance frequency of 25-30 kHz which corresponds to a membrane radius of 450-500μm. To observe the change of the first resonance frequency with different membrane radius values more clearly, the frequency region of interest is plotted as shown in Figure 2.5.

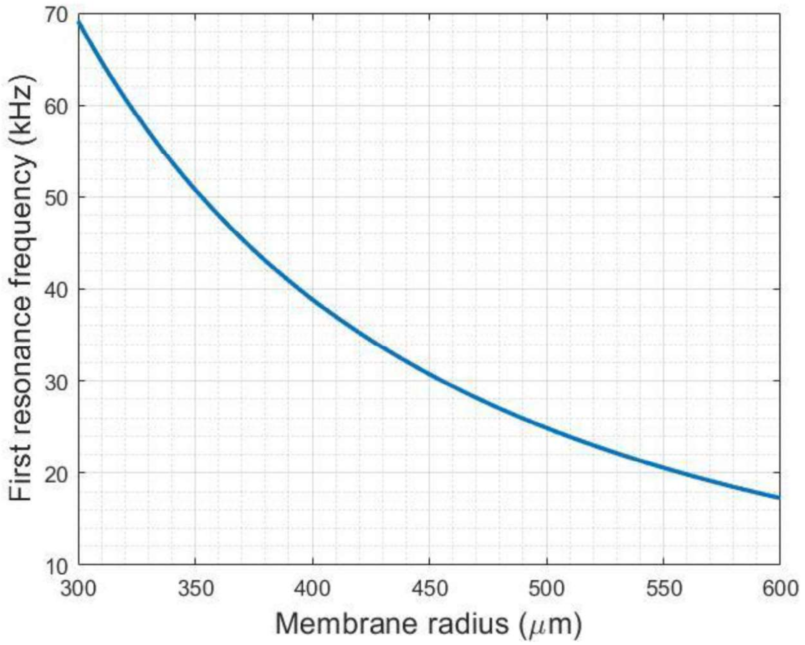

Figure 2.4. First resonance frequency of a circular membrane for different radius values.

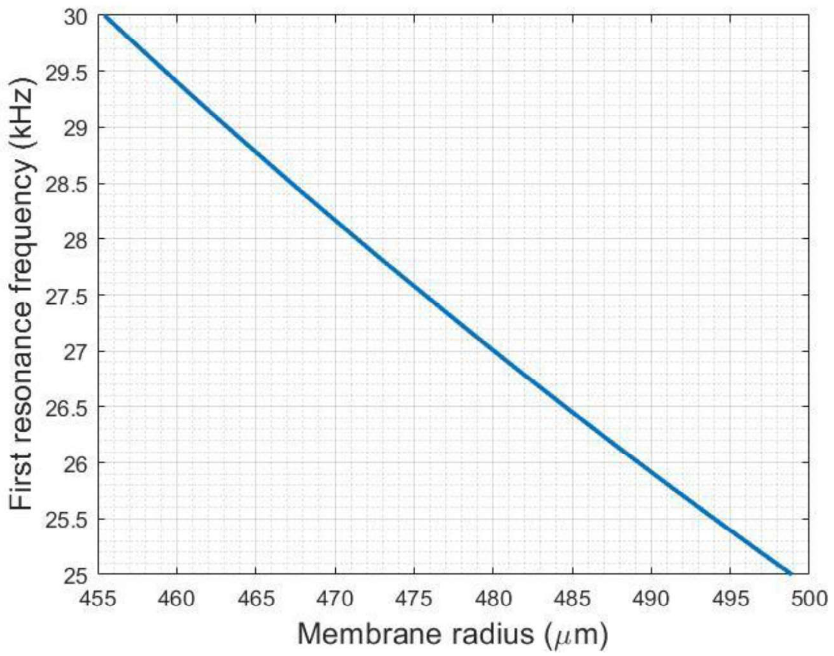

Figure 2.5. First resonance frequency of a circular membrane for different radius values in the frequency region of interest (25-30 kHz).

It is observed that the characteristics is almost linear for the frequency range of 25-30 kHz. Since POLYMUMPS will be used for microfabrication, there will be air holes on the membrane.

We may represent the resonance frequency of the membrane as

$$f = \frac{1}{2\pi}\sqrt{\frac{k}{m}} \tag{2}$$

where k is the spring constant and m is the mass. Considering the holes in the design, spring constant and mass decreases approximately by the same amount. Therefore, we may not expect significant change in the first resonance frequency due to holes.

2.3.2. Hole Design

The diameter of the membrane is set to 1000µm and another design parameters of the membrane are the hole diameter and the distance between the air holes. According to the design rules, to obtain perfect oxide etch under the membrane, any point on the membrane must be reachable by any of the air holes with a maximum of 15µm distance. This problem is represented as in Figure 2.6.

d_{HOLE} is the diameter of an air hole and $d_{HOLE\text{-}TO\text{-}HOLE}$ is the distance between the centers of two air holes. Since the membrane is fully symmetric, the air hole dimensions and the distances between any two air holes are the same anywhere on the membrane. Therefore, there are only two variables in hole design.

Due to the symmetry, centers of neighboring air holes generate an equilateral triangle. The geometric problem can be represented

$$(d_{HOLE-TO-HOLE}) * \frac{\sqrt{3}}{2} * \frac{2}{3} - \frac{d_{HOLE}}{2} \lesssim 15\mu m \tag{3}$$

$$2d_{HOLE-TO-HOLE} - \sqrt{3}d_{HOLE} \lesssim 30\sqrt{3}\mu m \tag{4}$$

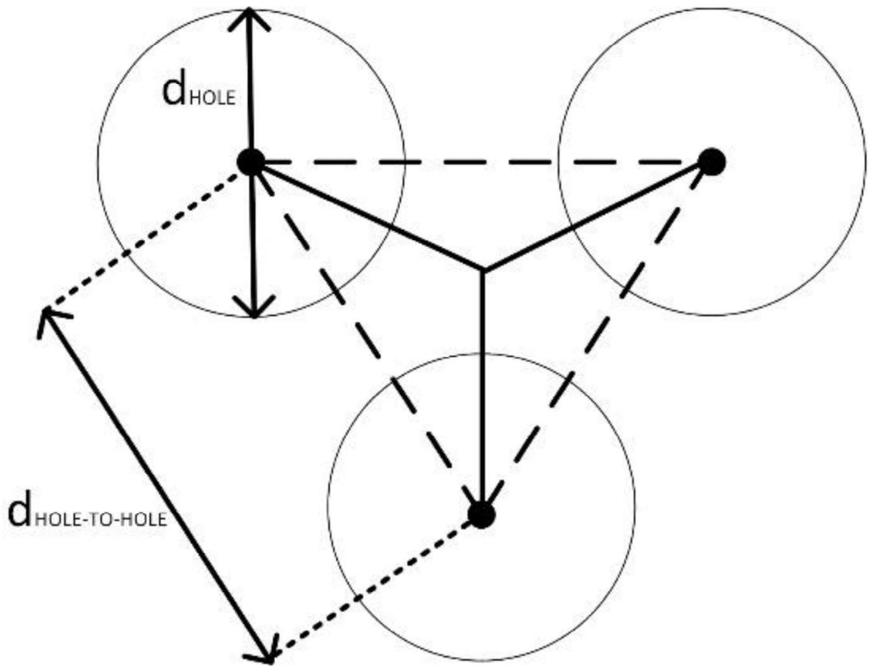

Figure 2.6. Hole arrangement problem.

One constraint on the dimensions is represented as in (4). Another objective of hole design is to maximize the fill factor (FF). As the area filled with polysilicon increases, the reflective area also increases. FF is given by Equation – (5)-(6).

$$FF = \frac{d_{HOLE-TO-HOLE}{}^2 * \frac{\sqrt{3}}{4} - \pi \frac{(\frac{d_{HOLE}}{2})^2}{2}}{d_{HOLE-TO-HOLE}{}^2 * \frac{\sqrt{3}}{4}} \tag{5}$$

$$FF = 1 - \frac{\pi}{2\sqrt{3}} (\frac{d_{HOLE}}{d_{HOLE-TO-HOLE}})^2 \tag{6}$$

To set a limit for FF, it is aimed to obtain 50 % FF such that at least 50 % of the light will be reflected from the membrane surface. By setting this limit, this constraint can be represented as

$$\frac{d_{HOLE}}{d_{HOLE-TO-HOLE}} < 0.75 \tag{7}$$

This optimization problem is solved by setting $d_{HOLE} = 36\ \mu m$ and $d_{HOLE-TO-HOLE} = 50\ \mu m$. This optimization also includes the safety margins for the microfabrication. For this case, FF is 53 % and the maximum distance between any point on the membrane and an air hole is 11µm with 27 % safety margin.

CHAPTER 3

PROCESS DEVELOPMENT OF THE MEMS MEMBRANE

According to the design rules of POLYMUMPS and the theoretical analysis of a circular membrane, microfabrication masks are designed. In the design, POLY0 and POLY1 polysilicon layers of the POLYMUMPS process are used as carriers of the membrane and POLY2 is used as the membrane material. The membrane, POLY2 layer, is shaped with air holes. This structure is called the meshed-structure. Then, metal is coated on top of the membrane. The purpose of metal is to achieve an optically reflective surface for the laser light coming from the fiber optic cable. The metal layer is also shaped with air holes, with diameter larger than the diameter of the air holes of POLY2, such that no fabrication problem can occur.

3.1. Microfabrication Mask Design

There are 12 masks to design in POLYMUMPS process, namely, POLY0, HOLE0, ANCHOR1, DIMPLE, POLY1, HOLE1, POLY1-POLY2-VIA, ANCHOR2, POLY2, HOLE2, METAL, HOLEM [13].

3.1.1. POLY0 and HOLE0 Masks Design

POLY0 and HOLE0 masks are used to shape the first polysilicon layer of the process, POLY0. There is no need for air holes in the first polysilicon layer since POLY0 layer will not be used to create closed volumes in the design. Therefore, HOLE0 mask will be left empty. On the other hand, POLY0 mask is used. This mask is a light mask and therefore, the regions to preserve POLY0 layer should be indicated. POLY0 layer is the first carrier for the membrane on which POLY1 and POLY2 will be grown later in the process.

POLY0 layer will also be used as the electrical polysilicon layer. During the test of the membrane, electrical connections are needed, one ground and one signal connection is needed. The membrane itself can be used as the signal connection since it is electrically short circuited with POLY1 and POLY0 via the outer carriers. The ground connection is utilized by placing a POLY0 circle to the center of the design with dimeter of 900μm. The ground connection is connected to 4 electrical pads to minimize the series electrical resistance. The signal connection is also connected to 4 electrical pads due to the same reason. The overall POLY0 mask design is as in Figure 3.1.

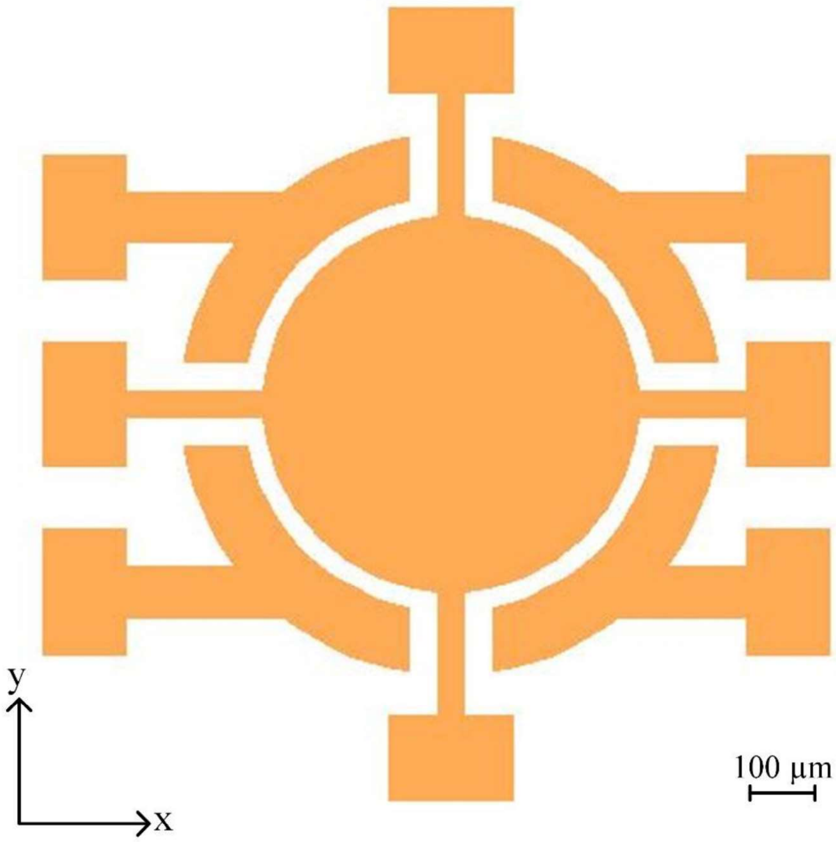

Figure 3.1. POLY0 microfabrication mask. Support, electrical connection pads, electrical polysilicon lines and electrical ground layer areas.

3.1.2. ANCHOR1 Mask Design

After POLY0 and HOLE0 masks are used to shape the first polysilicon layer, POLY0, the first oxide layer is grown on top of the wafer. This oxide layer is sacrificial and will be etched at the end of the process. ANCHOR1 mask is used to shape this first oxide layer. ANCHOR1 mask is a dark mask, in other words, in this mask, the regions that the designer want to etch should be indicated in ANCHOR1 mask. The purpose of this mask is to etch the oxide regions that the designer wants to grow POLY1 directly on top of POLY0. Since POLY0 and POLY1 layers are carriers for the POLY2 membrane layer, POLY1 should directly be grown on POLY0. Therefore, the anchor regions are indicated as in Figure 3.2. Here, the dashed parts indicate the ANCHOR1 mask regions where the oxide will be etched. On those regions, POLY1 layer will be grown directly on POLY0 layer.

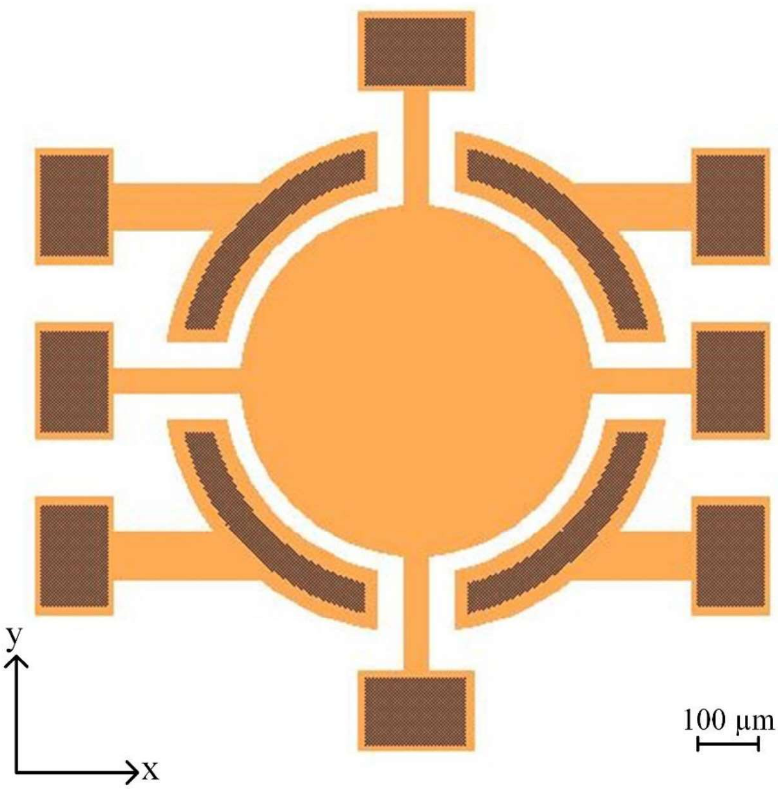

Figure 3.2. ANCHOR1 microfabrication mask (grey regions). Electrical connection pads and support areas.

3.1.3. DIMPLE Mask Design

Dimples are used to minimize the contact surface of the two layers, in this design POLY2 and POLY0. The first oxide is etched for 0.75µm on the areas indicated by DIMPLE mask. Since the membrane is fully symmetric, dimples are also placed symmetrically. The locations of the dimples are decided according to the positions of POLY2 etch holes. HOLE2 mask will be discussed later in the process, but the dimples are placed on the gravity center of the triangle that is formed by the centers of three neighboring etch holes. The placement can also be visualized by inspecting the hole design problem, in Figure 2.6. Dimples are placed at the gravity centers of such triangles as in Figure 2.6.

On electrical pad regions there is no need for dimples since in these areas, there is no moving component, all layers are put on top of each other. DIMPLE mask is as in Figure 3.3.

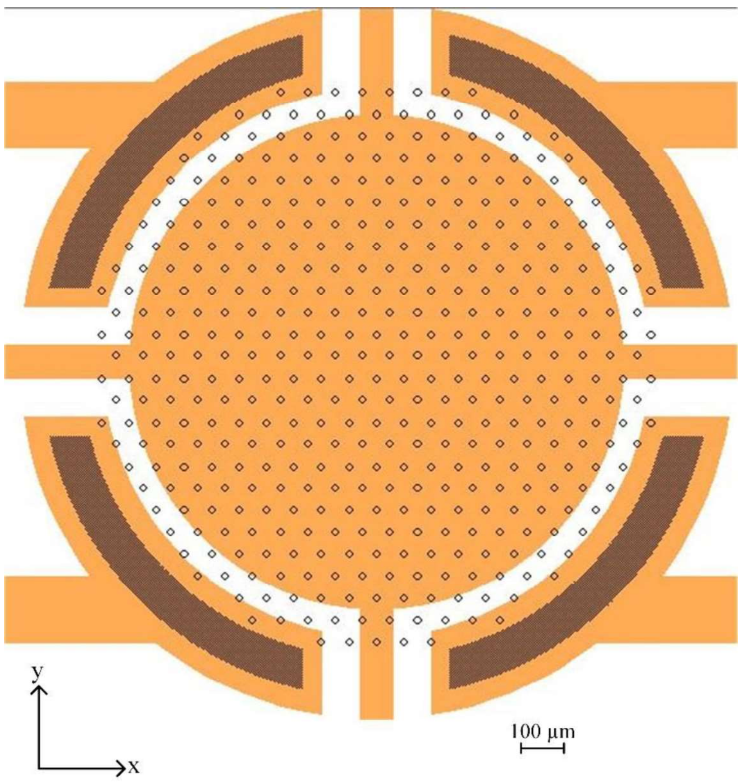

Figure 3.3. DIMPLE microfabrication mask. 0.75 µm deep small holes in the first oxide layer.

3.1.4. POLY1 and HOLE1 Masks Design

POLY1 and HOLE1 masks are used to shape the second polysilicon layer, POLY1. The main idea of these masks are the same as POLY0 and HOLE0. There is no need for air holes in POLY1 layer similar to POLY0 layer. POLY1 layer is sued as the second carrier part which will directly be grown on POLY0 layer. İnitially, POLY1 layer is grown all over the wafer. Since there are etched oxide regions indicated by ANCHOR1 and DIMPLE masks, there etched regions will also be filled by POLY1. Then, this second polysilicon layer will be shaped according to POLY1 mask. This mask will indicate the regions that the designer wants to preserve POLY1 layer. POLY1 mask is as shown in Figure 3.4.

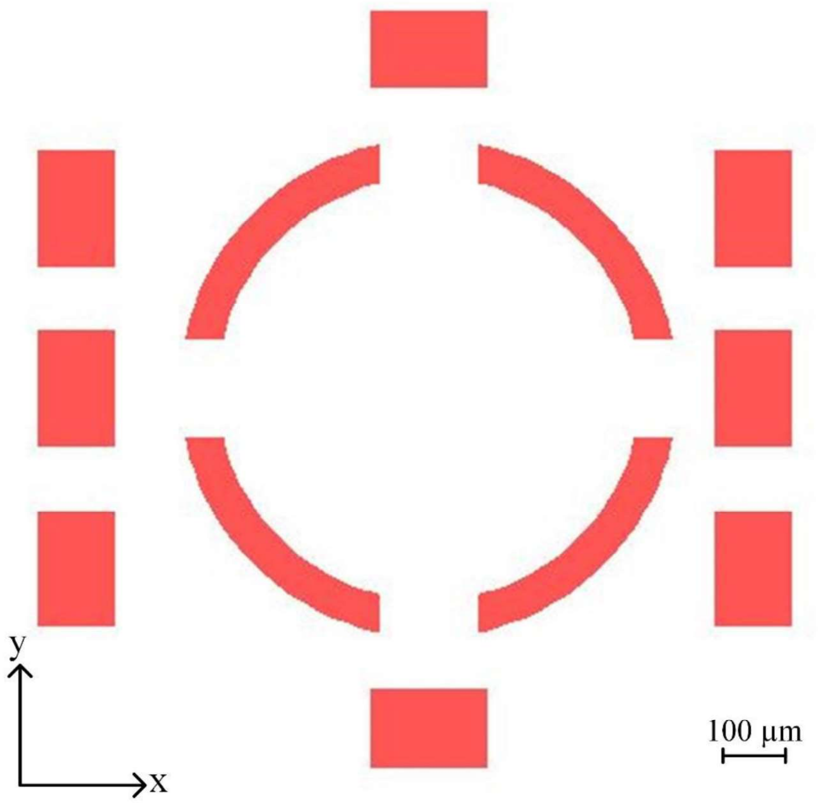

Figure 3.4. POLY1 microfabrication mask. Electrical pads and support layer areas.

The regions of POLY1 mask are given in Figure 3.4, but in order to understand the exact location of the mask relative to the previous masks, POLY0, ANCHOR1 and

POLY1 masks are illustrated together in Figure 3.5. The red regions represent POLY1 layer. The ANCHOR1 and DIMPLE oxide holes are filled by POLY1 layer. In this way, POLY1 is positioned on top of POLY0 layer and the carriers are obtained. Another important thing about the POLY1 layer is that POLY1 layer thickness will determine the maximum amount of deflection of the membrane. There is ground connection utilized by POLY0 layer under the membrane and the only air gap between the membrane and this POLY0 ground connection regions is the thickness of POLY1. Therefore, proper growth of POLY1 on the wafer is highly critical for the operation of the membrane.

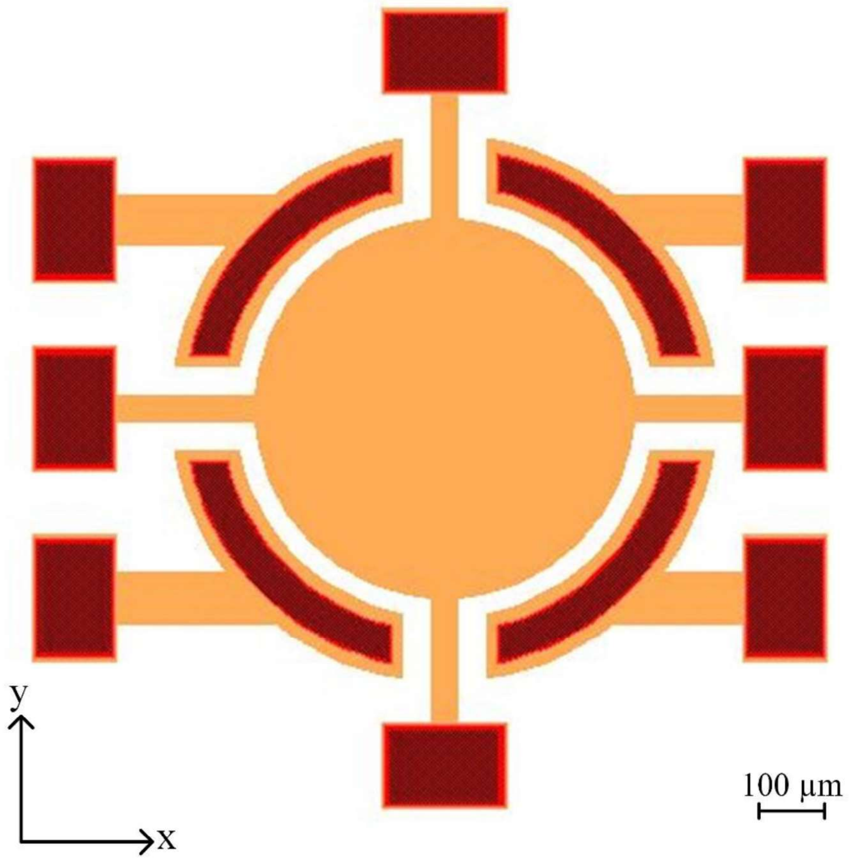

Figure 3.5. POLY0(orange), ANCHOR1(grey) and POLY1(red) microfabrication masks on top of each other.

3.1.5. POLY1-POLY2-VIA Mask Design

After the POLY1 layer processing part, the second oxide layer is grown on top of the wafer. This layer is the second sacrificial layer that will be etched at the end of the process. Also, on top of this second oxide layer, the third polysilicon layer, POLY2, will be grown. Therefore, the designer should indicate the regions where POLY2 will be directly grown on POLY1. In this membrane design, these regions are the carrier regions, the outer, non-moving polysilicon regions. Since POLY1-POLY2-VIA mask is a dark mask, the regions that the second oxide will be etched are indicated in this mask. POLY1-POLY2-VIA mask is given together with POLY1 mask as in Figure 3.6 in order to visualize the operation better.

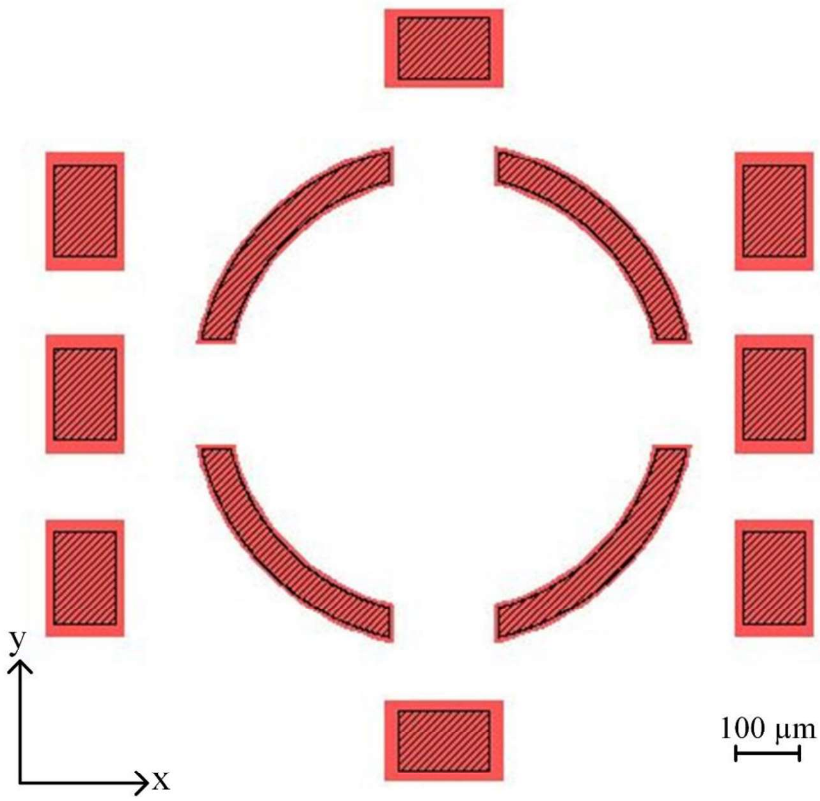

Figure 3.6. POLY1(red) and POLY1-POLY2-VIA(shaded) microfabrication masks.

The dashed regions in Figure 3.6 indicate POLY1-POLY2-VIA regions and the red regions indicate the POLY1 regions. Another important point with this mask is related to the DIMPLE mask. In the standard form, DIMPLE mask generates holes on the first oxide and these holes prorogate through the second oxide. However, the sharpness of these holes may be disturbed due to thermal processing. POLYMUMPS suggests the designers that want dimples for POLY2 layer to draw the dimple holes also on POLY1-POLY2-VIA mask. By this way, the second oxide is etched for 0.75µm in dimple regions. This process will guarantee the utilization of dimples and the dimple holes are directly reflected to the top surface of the second oxide layer. POLY1-POLY2-VIA mask with these dimple holes are given as in Figure 3.7.

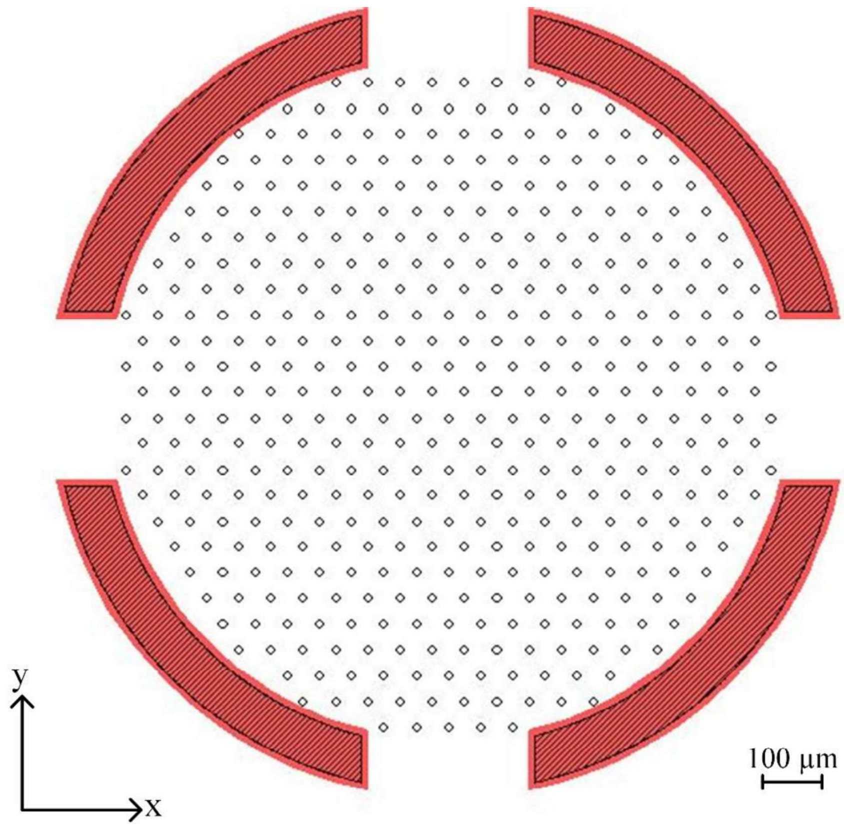

Figure 3.7. POLY1-POLY2-VIA microfabrication mask, with small holes which overlap with DIMPLE mask to strengthen the utilization of dimples for the upper layers.

3.1.6. ANCHOR2 Mask Design

ANCHOR2 mask is used to indicate the regions where the second oxide and the first oxide will be etched such that POLY2 will be grown directly on POLY0 or nitride layers. In the design of the membrane, there is no need for such mask; therefore, it is not used in the process.

3.1.7. POLY2 and HOLE2 Masks Design

POLY2 and HOLE2 masks are used to shape the third polysilicon layer, POLY2. This is the most important layer of the process since POLY2 layer will be the membrane itself. First, the third polysilicon layer is grown all over the wafer and the oxide holes generated by POLY1-POLY2-VIA masks will be filled by POLY2. In addition to the carrier regions, the dimple holes are filled by POLY2. The top surface of the second oxide is also covered by POLY2. POLY2 mask is used to shape this POLY2 layer. Different from POLY0 and POLY1 masks, the central part of this layer is not etched since this central part will form the membrane itself. POLY2 mask is as in Figure 3.8.

In order to visualize the position of POLY2 mask relative to the other masks, POLY2 mask is given together with all of the other masks so far in Figure 3.9. In Figure 3.9, the central portion is left only with POLY2 layer to form the membrane. The grey regions indicate the POLY2 layer where the red regions indicate POLY1 and the orange regions indicate POLY0.

At this point, there is a need for hole masks since in the central part of the design, under the membrane, there are oxide layers that should be etched. For that purpose, there is a need for etch holes in POLY2 layer and HOLE2 masks is designed.

The hole diameter and the arrangement of the holes are analyzed in Section 2.3.2 and HOLE2 mask design is performed according to the outcomes of this analysis. HOLE2 mask is given in Figure 3.10 together with POLY2 mask.

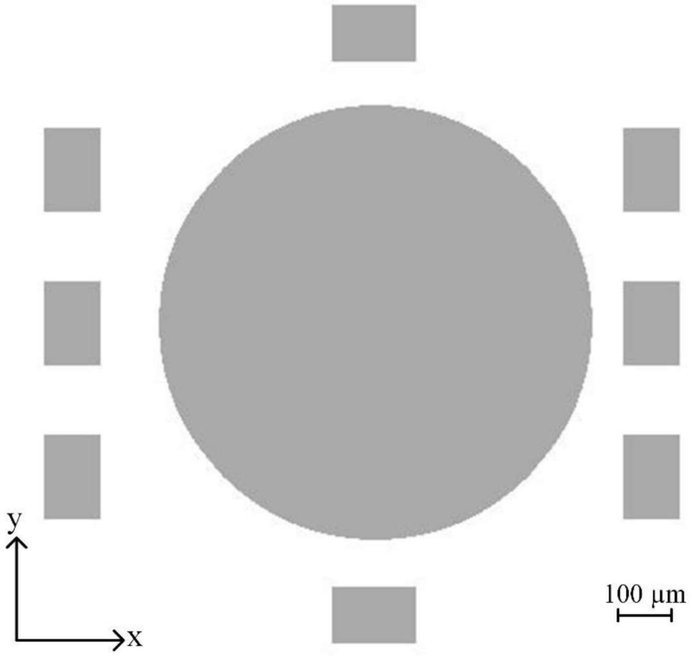

Figure 3.8. POLY2 microfabrication mask.

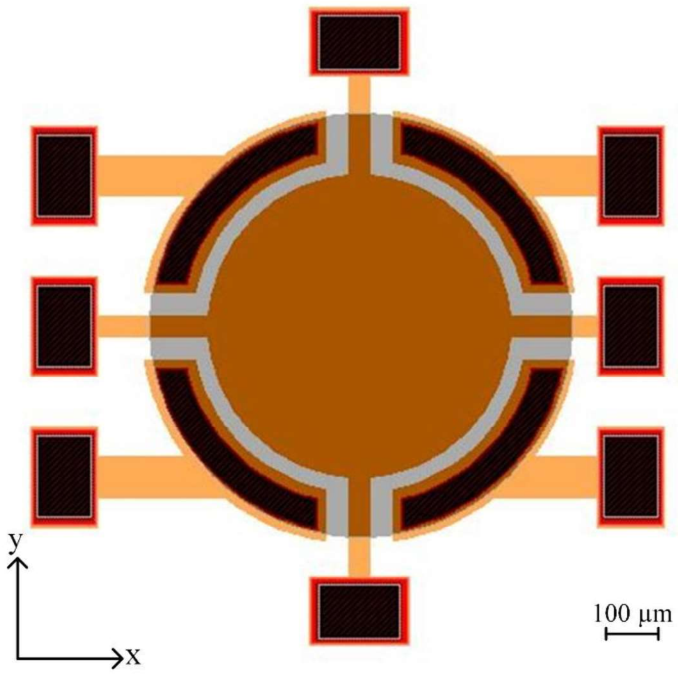

Figure 3.9. POLY0(orange), ANCHOR1(dark grey), POLY1(red), POLY1-POLY2-VIA(shaded) and POLY2(grey) microfabrication masks.

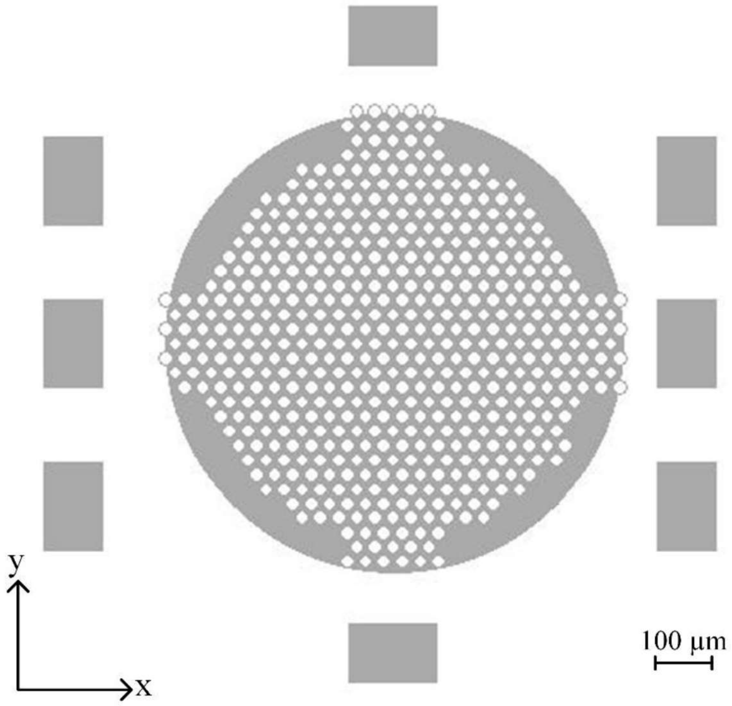

Figure 3.10. POLY2 and HOLE2 microfabrication masks.

During placement of the etch holes, symmetry was violated at the boundary regions since at these regions, the mathematical study of hole design is no longer valid. In other words, in the carrier polysilicon regions, the outer shell, there is oxide on the one side while there is no oxide on the other side of the boundary. Therefore, the hole arrangements in the outer regions of POLY2 performed according to the Design Rule Check (DRC). Nevertheless, since these regions are barely moving, it can be assumed that the symmetric operation of the membrane is not disturbed.

3.1.8. METAL and HOLEM Masks Design

After all of the polysilicon layers are located on the wafer and shaped properly, metal is sputtered on top of the wafer. Metal is critical for the membrane design since there is a need for an optically reflective surface and polysilicon is not sufficient. In the process, the wafer is first coated with photoresist and then, the photoresist is patterned by photolithography according to METAL and HOLEM masks. Finally, the lift-off method is used to shape the metal surface. HOLEM mask is used only for the designer similar to other hole masks, but it dramatically improves the clearness of the mask design. The METAL mask is given in Figure 3.11 together with POLY2 and HOLEM mask is shown in Figure 3.12 together with POLY2, HOLE2 and METAL masks.

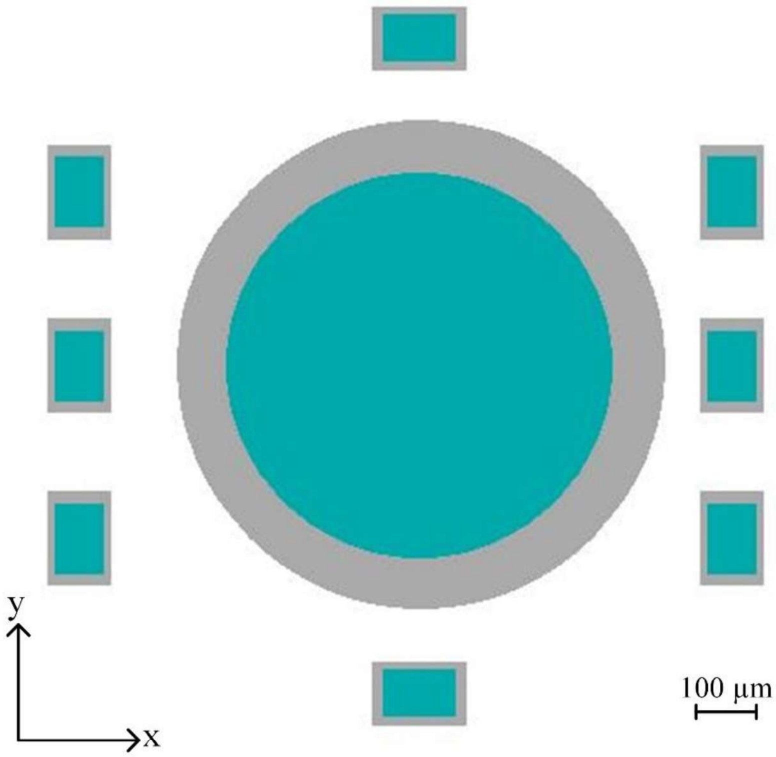

Figure 3.11. POLY2(grey) and METAL(blue) microfabrication masks.

The blue regions indicate the metal regions and the grey regions indicate POLY2 regions. The dimeter of metal holes is larger than the diameter of POLY2 holes according to the design rules. Otherwise, the metal would be left on the oxide under POLY2 holes and it would cause problems during the sacrificial oxide etch.

At the end of the process, the oxide layers are etched by wet etch followed by dry etch. Hence, The POLY2 layer is free to move in upwards and downwards directions supported by the polysilicon carrier outer shells. Also, there are electrical connection pads which are designed for the electrical characterization of the membrane.

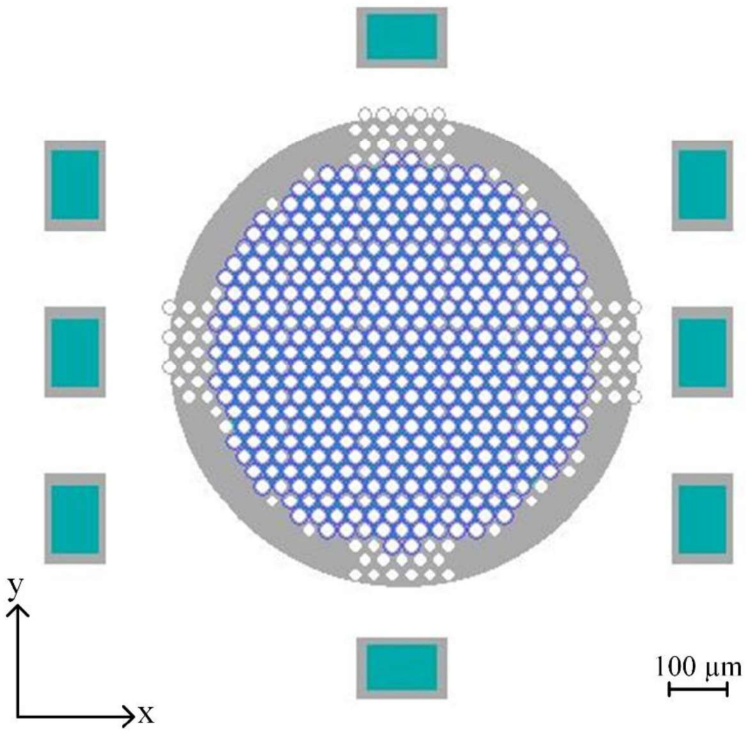

Figure 3.12. POLY2(grey), HOLE2, METAL(blue) and HOLEM masks.

3.2. Three Dimensional (3D) and Two Dimensional (2D) Models of the Design

Before submitting the microfabrication masks to POLYMUMPS, it is desired to visualize the membrane in three dimension to verify the mask design. For that purpose, SOFTMEMS 3D Render extension of L-Edit software is used.

First, the process sequence is defined in the software; the layers and the types of growth or etch of each layer should be entered by the designer. The sequence and the physical parameters should also be entered to the software. SOFTMEMS 3D Render extension only generates the geometric result of the process, the probable errors of the real process or the secondary effects such as the stiction of the membrane to the wafer due to wet etch are not considered.

After the process is defined properly, the 3D model of the design is obtained as in Figure 3.13-15. The layers are observed on the 3D model. Each layer is represented by different color. The membrane has meshed-structure with air holes and the upper surface of the membrane is coated with the metal layer. The air holes of the metal layer are also represented. In Figure 3.14, the cross-sectional view is represented and in Figure 3.15, the oblique view of the design is given which clearly verifies the design. The oxide holes created by ANCHOR1 and POLY1-POLY2-VIA are visible in which POLY1 and POLY2 has grown, respectively.

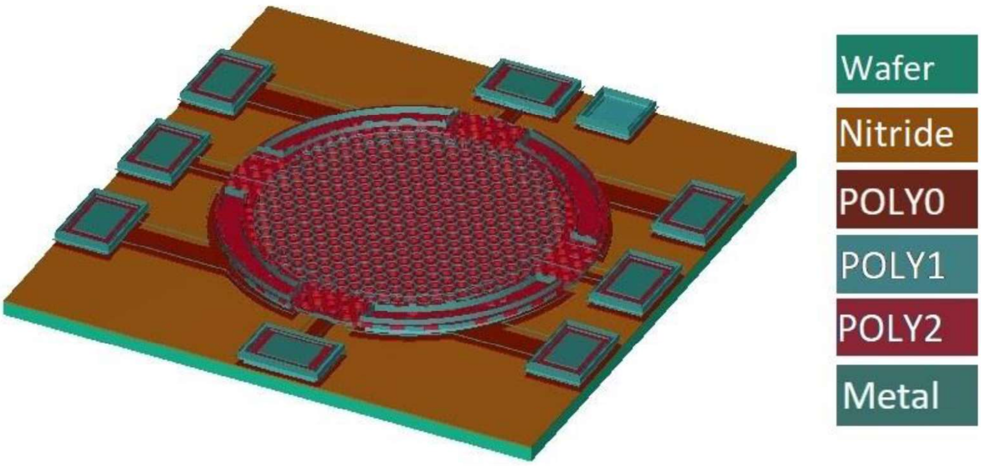

Figure 3.13. 3D model of the membrane.

In this model, DIMPLE mask is not executed since it increases the computation time and time-out occurs. To overcome this issue and verify the DIMPLE mask, a small portion of the design is modelled in 3D as in Fig. 3.16.

In Figure 3.16 (a), the 3D model of a small portion of the design taken from the central part is represented and in Figure 3.16 (b), the cross-sectional view is given. The dimples can be observed in Figure 3.16 (b). These dimples decrease the contact surface between the membrane and the layer underneath it which will prevent the membrane from sticking to the wafer (due to adhesive forces) during wet etch.

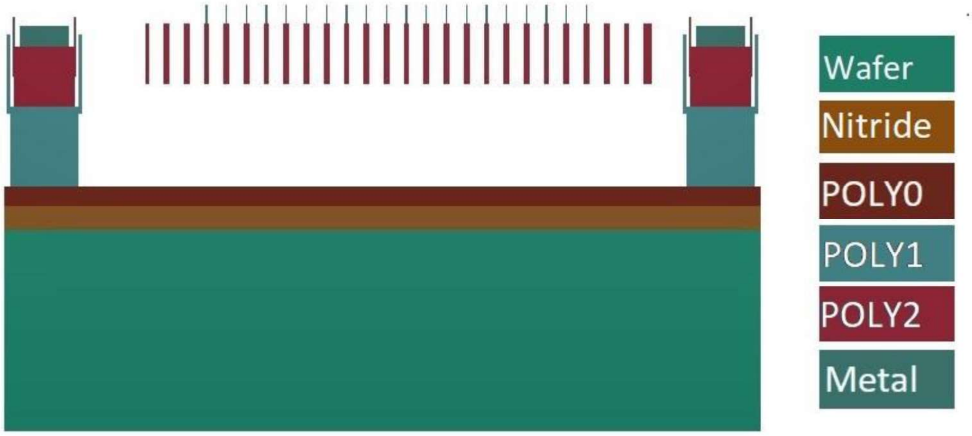

Figure 3.14. Cross-sectional view of the 3D model of the membrane.

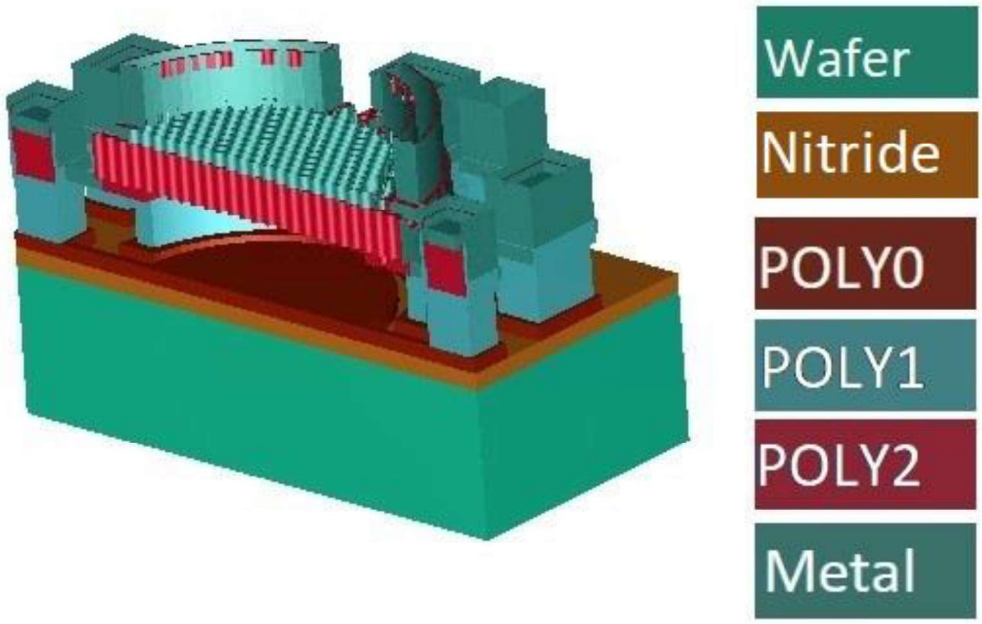

Figure 3.15. Oblique view of the 3D model of the membrane.

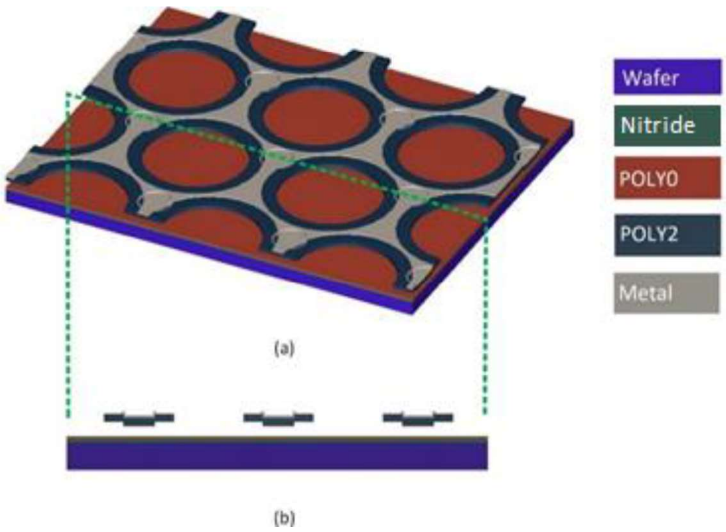

Figure 3.16. (a) Oblique, (b) cross-sectional view of the 3D model of a small portion of the design

In Figure 3.14 and Figure 3.16 (b), the two dimensional cross-sectional model of the design is visualized. To inspect the cross-sectional view in more detail and with the real dimensions, the view in Figure 3.17 is obtained and the values of the representative dimensions are given in Table 3.1.

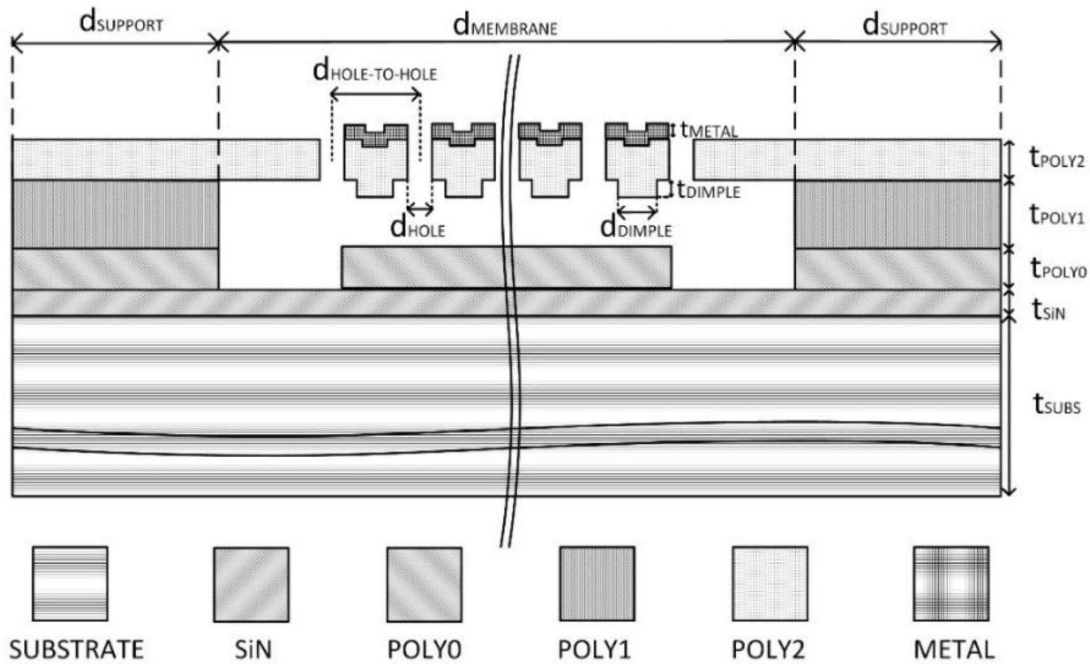

Figure 3.17. Cross-sectional view of the membrane design.

Table 3.1. *Values of the representative dimensions of the design.*

Dimension parameter	Value
Membrane diameter ($d_{MEMBRANE}$), µm	1000
Support length ($d_{SUPPORT}$), µm	150
Hole-to-hole diameter ($d_{HOLE-TO-HOLE}$), µm	50
Dimple diameter (d_{DIMPLE}), µm	12
Hole diameter (d_{HOLE}), µm	36
Metal thickness (t_{METAL}), µm	0.51
POLY2 thickness (t_{POLY2}), µm	1.5
Dimple thickness (t_{DIMPLE}), µm	0.75
POLY1 thickness (t_{POLY1}), µm	2.0
POLY0 thickness (t_{POLY0}), µm	0.51
SiN thickness (t_{SiN}), µm	0.61
Substrate thickness (t_{SUBS}), µm	>650

In Figure 3.17, the final design is modelled and the fabricated designs are expected to be the same shape as this model with small microfabrication errors. The effects of dimples and their propagation through the surface are also represented.

3.3. Microfabricated MEMS Membrane

The microfabrication masks are submitted to POLYMUMPS and the microfabricated designs are received. The devices are inspected under the microscope for any macro errors. The designs seem to be microfabricated without major errors as in Figure 3.18.

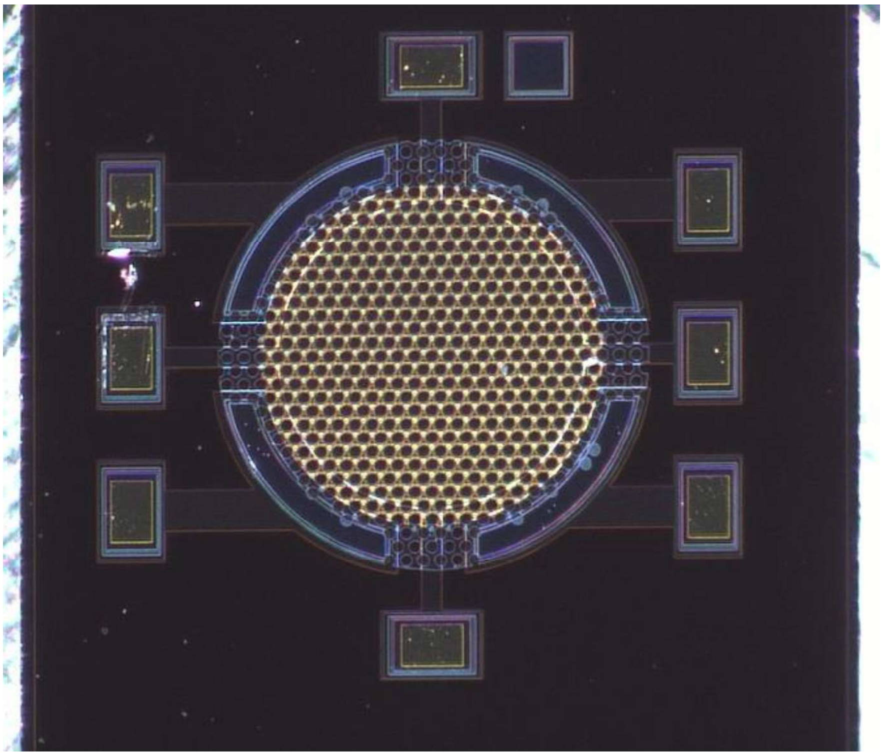

Figure 3.18. Microscope view of the microfabricated design.

The electrical connection pads are placed properly and the air holes on the membrane, POLY2 layer of the design, are utilized according to the microfabrication masks.

CHAPTER 4

ELECTRICAL AND OPTICAL CHARACTERIZATION SETUPS

After the first inspection of the microfabricated design, it is aimed to characterize it and verify its performance. For that purpose, two different methods are used. First, electrical impedance characterization is performed. The resonance frequencies of the device can be obtained by series capacitance and resistance measurements under different bias voltages. Secondly, the laser vibrometer setup is employed. With this optical setup, a point by point frequency response of the membrane can be obtained. In other words, any point on the membrane can be characterized. By this way, in addition to the resonance frequency analysis, spatial response of the membrane to any input can be analyzed. Modal shapes of each resonance can be obtained and the symmetry of the device can be verified.

4.1. Electrical Measurement Setup

For the electrical characterization of the membrane, impedance and network analyzer (Keysight Technologies 5061B) is used. This device is used for the characterization of high frequency operating circuits. For that purpose, s-parameter measurement port is used. However, for the characterization of the membrane of fiber optic MEMS microphone, low frequency measurement is desired. In the instruction manual of the device, it is suggested to use LF-out port of the device and use the power splitter (Agilent 11667L) in the shunt-through configuration. The suggested setup for low frequency measurement is as in Figure 4.1. The critical supplementary hardware for this measurement is the power splitter and its technical specifications are given in Table 4.1 [36].

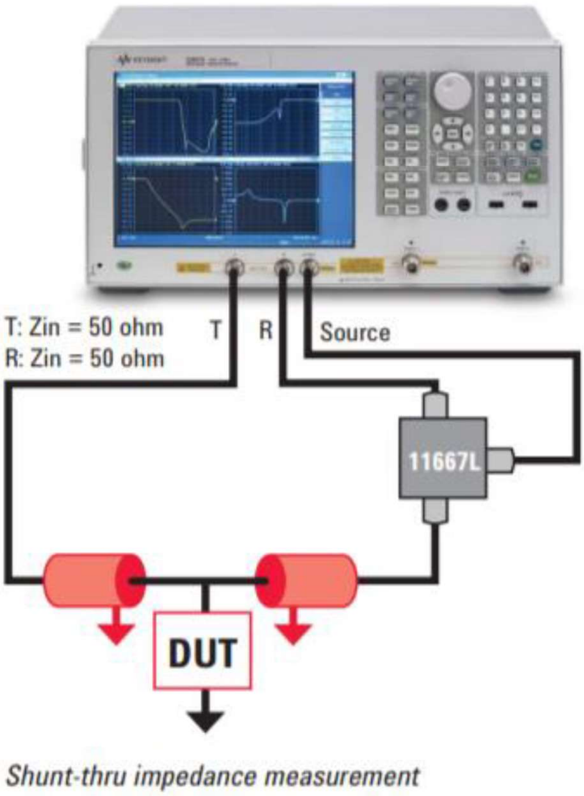

Figure 4.1. LF-out measurement connections [36].

Table 4.1. *Specifications of Agilent 11667L power splitter [36].*

Specifications	Keysight 11667L
Frequency Range	DC to 2 GHz
Connector	BNC(f)
Insertion Loss above 6 dB (max)	DC to 100 MHz : 0.2 dB
	100 MHz to 2 GHz : 0.6 dB
Isolation (Min)	DC to 2 GHz : 11dB
Return Loss (SWR) Typical	Input : 18 dB (1.3)
	Output : 11 dB (1.78)

Amplitude Tracking (Max)	DC to 100 MHz : 0.1dB
	100 MHz to 2 GHz : 0.2 dB
Phase Tracking (Max)	DC to 100 MHz : 1 deg
	100 MHz to 2 GHz : 3 deg
Maximum Input Power	500 mW

From Table 4.1, it is clear that power splitter is operating in the frequency range of 0 – 100 kHz. The reason why s-parameter measurement yields faulty results is that the calibration of this port is appropriate for high frequencies (1-10 GHz) whereas the frequencies of interest for the fiber optic MEMS microphone is very small compared to the calibration of high frequencies.

The setup for the measurement is as shown is Figure 4.2 [37].

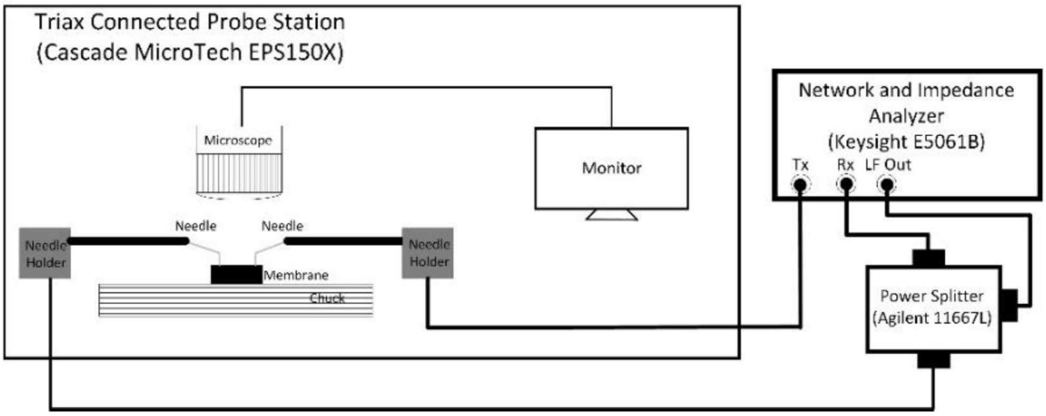

Figure 4.2. Electrical measurement setup [37].

To perform low noise measurements, triax-connected probe station (Cascade MicroTech EPS150X) is used. To lower the noise in the system, tungsten needles (Cascade MicroTech PTT-120-/4-25) are preferred in the probe station. The MEMS design on the chuck of the probe station and the view of it under the microscope are as shown in Figure 4.3 [37].

In order to detect any resonance frequency in the range of 1 kHz -100 kHz, and verify the operation of the membrane, series capacitance and series resistance measurements are taken from impedance analyzer in the electrical measurement setup. The settings of the impedance analyzer are as in Table 4.2 [37].

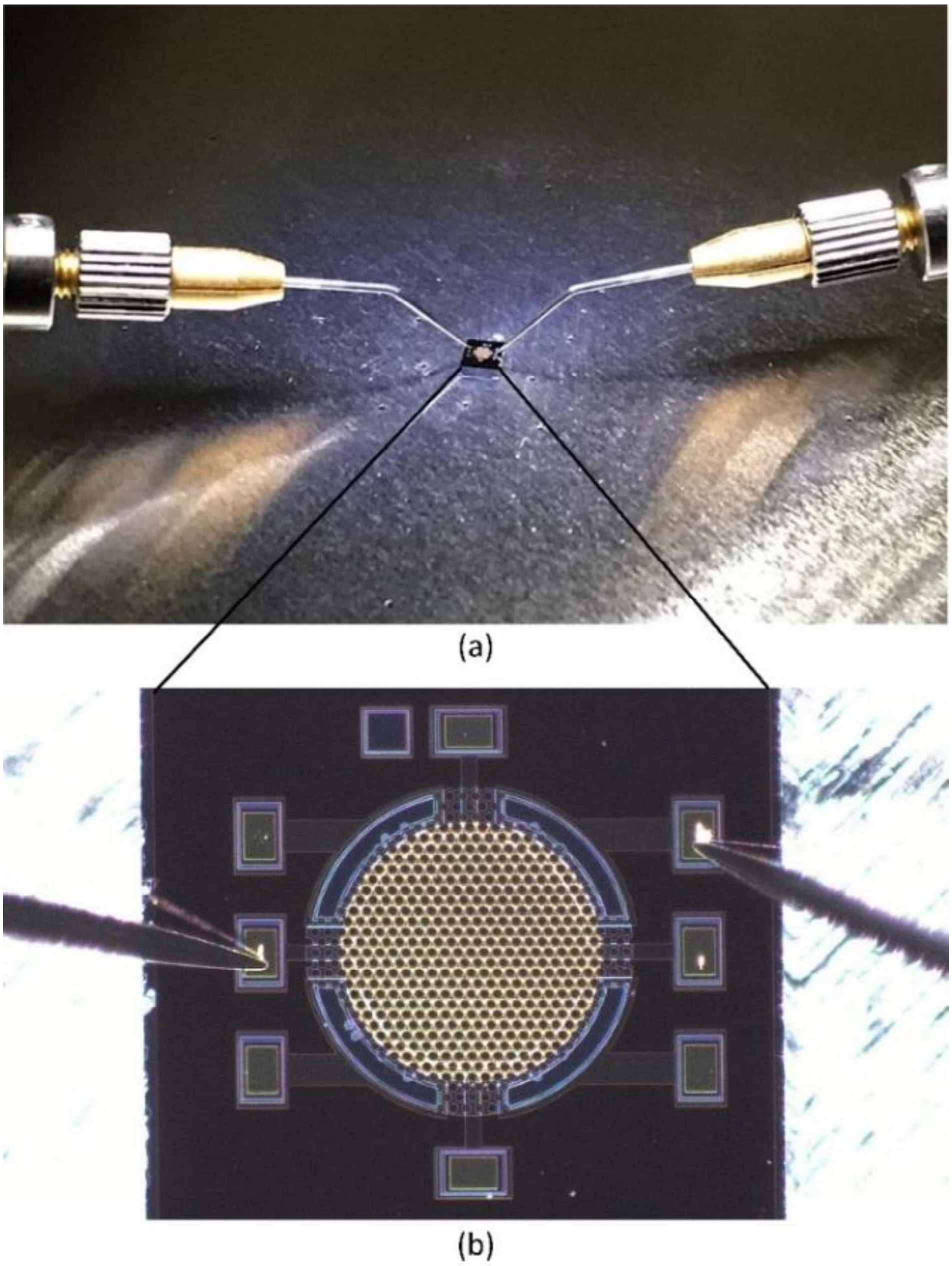

Figure 4.3. The view of the chip (a) on the chuck and (b) under the microscope of the probe station [37].

Table 4.2. *The settings of the impedance analyzer for the electrical characterization [37].*

Setting	Value
Frequency sweep range	1 kHz – 100 kHz
Intermediate Frequency Bandwidth (IFBW)	500 Hz
Averaging	32
Number of data points in the frequency range	1601
AC voltage	10 dBm
DC bias voltage range	0V – 3V

The impedance analyzer applies voltage across the device and measures the current. By this way the impedance of the device under test is realized and it is then decomposed to its real and imaginary components. The real component is the series resistance and the imaginary component is the series capacitance of the device.

$$Z = \frac{V}{I} = |Z|e^{j\theta} = |Z|cos\theta + j|Z|sin\theta \qquad (8)$$

$$R_s = |Z|cos\theta \qquad (9)$$

$$C_s = \frac{-1}{\omega|Z|sin\theta} \qquad (10)$$

The impedance analyzer sweeps the frequency and takes these measurements at each point. Averaging is also used to obtain more accurate results.

4.2. Optical Measurement Setup

Electrical characterization of the design gives the general response of the membrane to inputs at different frequencies and different bias levels. To investigate the properties of the design in more detail, optical characterization setup is used.

Optical measurement setup consists of the laser vibrometer (Polytec OFV5000), digital oscilloscope (Agilent DSO6014A), function generator (Agilent 33250A) and a personal computer with LabView software (National Instruments, Texas, USA) installed on it to control the hardware in the setup. Optical measurement setup is as shown in Figure 4.4. The settings of the optical measurement setup are as in Table 4.3 [37].

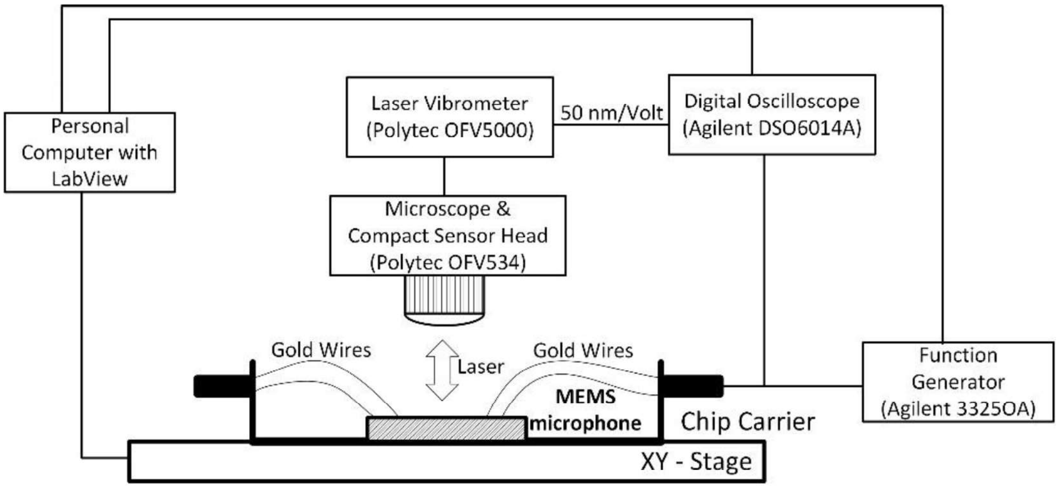

Figure 4.4. Optical measurement setup [37].

Table 4.3. *The settings of the signal generator for optical characterization [37].*

Setting	Value
Frequency sweep range	3 kHz – 150 kHz
AC voltage	100 mV_{pp}
DC bias voltage	1V

In the optical measurement setup, the membrane is excited electrically and the local responses on the membrane surface are measured with the laser light. The wavelength of the laser light in the system is 633 nm and the light can focus on a spot as small as 2μm allowing the system to take very fine measurements. The membrane and the laser source that generates and sends photons to the membrane generate an interferometer. As the membrane moves, the distance that the light travels changes and from the interferometer output, the deflection of the membrane can be determined from the phase shifts of the light. The utilization of light in the optical measurement setup makes it very critical for the verification of the operation of the membrane since the membrane will be used in a fiber optic MEMS microphone which detects the deflection of the membrane optically.

CHAPTER 5

CHARACTERIZATION OF THE MEMBRANE

5.1. Electrical Measurement Results and Discussion

During the characterization of the design through impedance analyzer, DC bias voltage is limited by 3V in order to avoid the collapse of the membrane on the ground plate. Collapse of the membrane results in the electrical short circuit of the membrane and the ground pad which may burn out the membrane due to high current.

The membrane design can be modelled as a parallel plate capacitor since it has two parallel plates and an air in-between them. The plates are circular and the dimensions are known form the design and the information from MEMSCAP. Since the membrane can be modelled as a parallel plate capacitor, electrical characterization is applicable. The capacitance of the membrane can be calculated by parallel plate capacitor capacitance for different cases.

$$C = \varepsilon \frac{A}{d} \tag{11}$$

where ε is the electrical permittivity of the material between two plates of the capacitor, this is $\varepsilon_0 = 8.85 * 10^{-12} F/m$ for air, A is the area of parallel plates, the smaller area is considered for the design which is the area of the ground pad, and d is the distance between two plates, which varies for different cases and different locations on the membrane. The theoretical series capacitance values under different conditions are given in Table 5.1.

Table 5.1. *The theoretical series capacitance for different conditions.*

Condition, Distance between the plates (d)	Capacitance Value (pF)
Electrical connection from POLY2, d = 2.00 μm	1.3678
Electrical connection from POLY2, d = 1.32 μm	2.0517
Electrical connection from POLY2, d = 1.00 μm	2.7356
Electrical connection from METAL, d = 2.00 μm	0.56959
Electrical connection from METAL, d = 1.32 μm	0.82931
Electrical connection from METAL, d = 1.00 μm	1.0742

In Table 5.1, six different conditions are considered. In the first three cases, it is assumed that the electrical connection of the membrane is taken from POLY2 layer. Under this condition, the distance between the membrane and the ground pad changes as the DC bias voltage varies. Therefore, three different distances are considered. After that, in the last three conditions, it is assumed that the electrical connection of the membrane is taken from METAL layer. Similarly, three different distances are considered due to the same reasons for the first three cases. The consideration whether the electrical connection comes from POLY2 or METAL layers depends on the applied frequency. Depending on different applied frequencies, the electrical connection may be taken from only POLY2, or only METAL.

From theoretical calculations, it is observed that the series capacitance value for any case is only a few pF. Under these circumstances, high quality measurement of exact series capacitance values become impossible due to the additional capacitive effects of the devices and cables. The measured series capacitance (C_s) and the series resistance (R_s) values in the frequency range of 1 kHz – 100 kHz are as shown in Figure 5.1 [37].

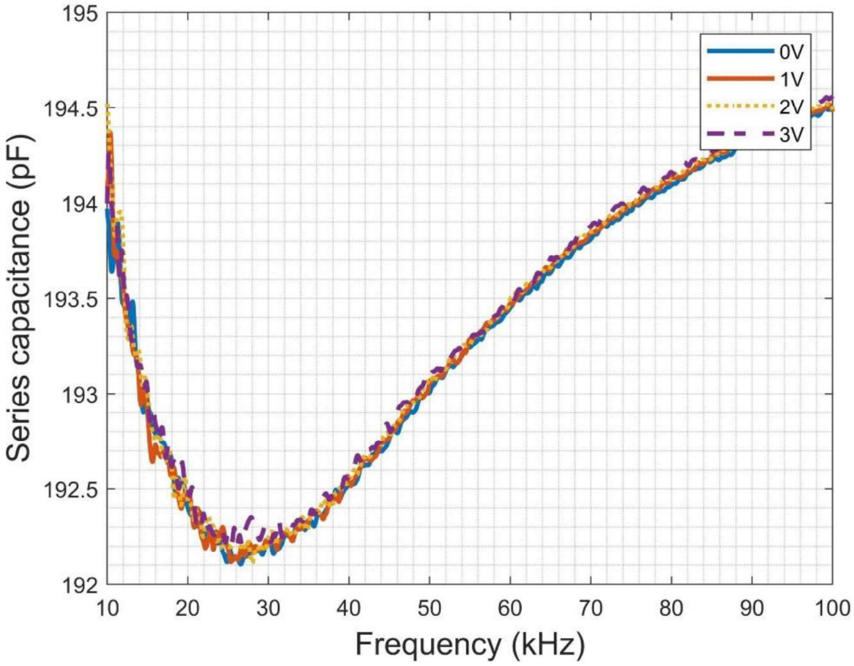

(a)

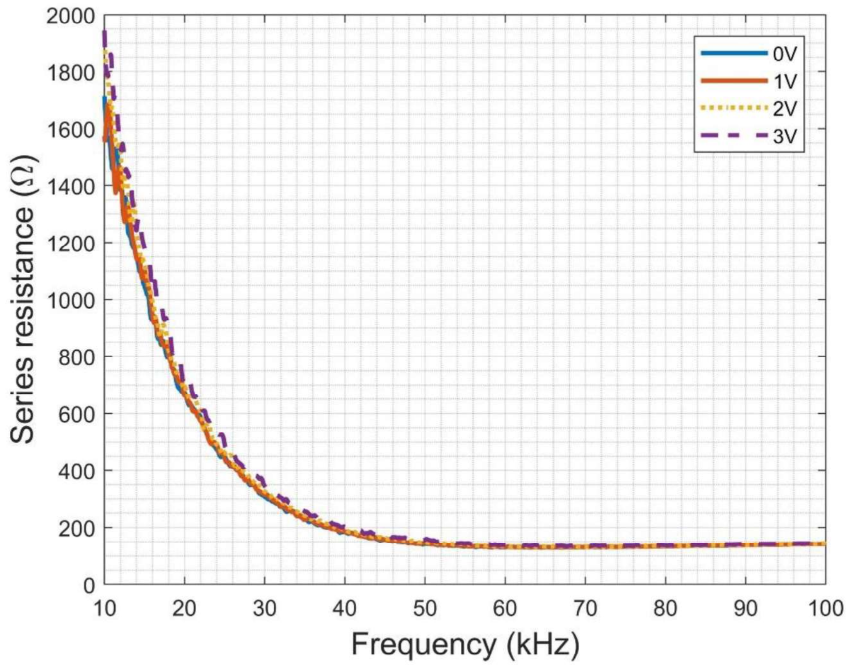

(b)

Figure 5.1. Measured (a) series capacitance, (b) series resistance as a function of frequency under different DC bias voltages [37].

In Figure 5.1 (a), it is observed that the series capacitance values vary between 192 pF – 195 pF range for different frequencies. In the theoretical calculations, the capacitance of the membrane was found to be in the order of few pF. The measured capacitance values are the combination of the capacitances of the membrane, electrical devices and the cables. It is also not possible to calibrate the system from the ends of the probes since the manufacturer does not supply reference loads for low frequency measurements and that's why the measured values are higher than the theoretical prediction of capacitance. It is also observed that the DC voltage does not change the value of the series capacitance in pF range which may be due to the small deflection of the membrane compared to the distance between the membrane and ground layer. In addition, the theoretical calculations yield a capacitance of few pF for the distances of 1-2 μm range between the plates. Applied DC voltage decreases this distance, but it is expected that the deflection is much smaller than this distance. Therefore, the effect of deflection due to applied DC bias cannot be observed on the capacitance measurements. The measured resistance values in Figure 5.1 (b) are relatively high due to the resistive lightly-doped polysilicon lines compared to the highly conductive metal.

5.2. Optical Measurement Results and Discussion

For the optical characterization of the membrane through the laser vibrometer, chip is placed on a chip carrier as shown in Figure 5.2 (a). The chip carrier has SMA type connection ports which are electrically connected to gold paths on the chip carrier. Electrical connection pads of the chip are electrically connected to these gold paths by wire bonding. The electrical connections and the gold paths on the chip carrier are shown in Figure 5.2 (b) [37].

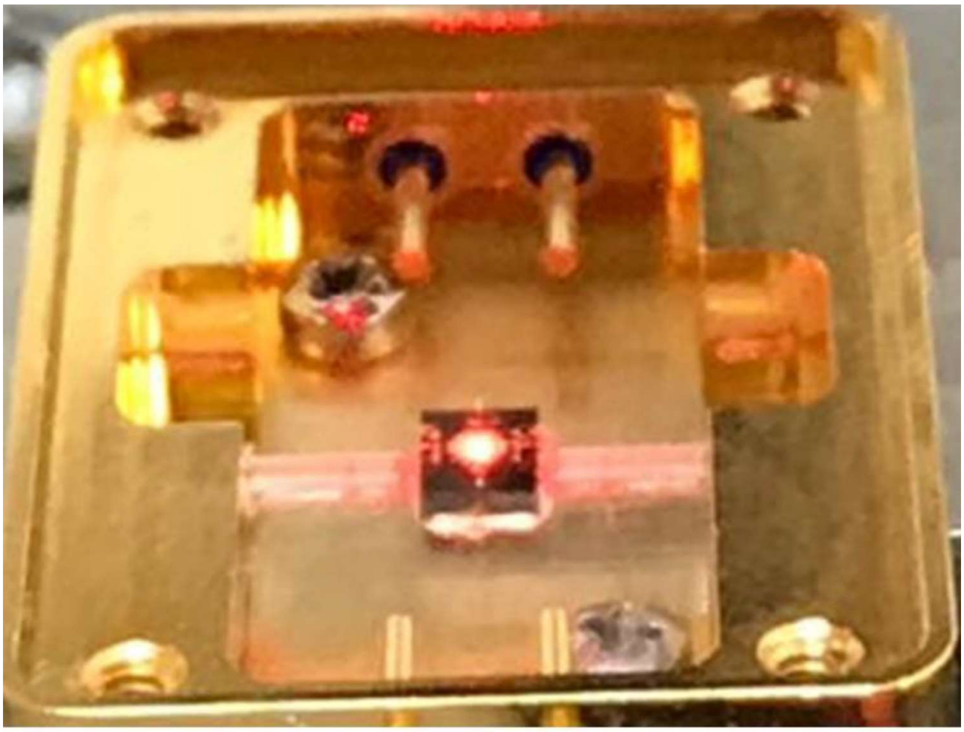

(a)

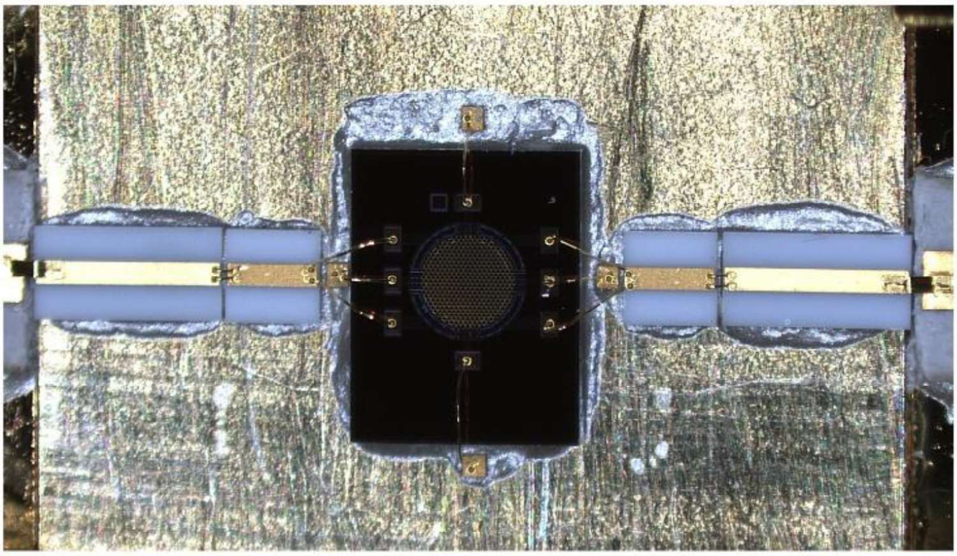

(b)

Figure 5.2. The view of the chip (a) on the chip carrier, (b) under the microscope [37].

Before optical measurements, setup is prepared properly. First, the chip carrier is placed on the chuck of the vibrometer and BNC to SMA connectors are used in order to connect the signal generator to the MEMS chip such that the membrane will be electrically excited. After that, the signal generator output and the laser vibrometer output are connected to the oscilloscope. The purpose of connecting the output of the signal generator to the oscilloscope is to use it as a triggering signal. Finally, the chuck of the vibrometer is controlled by LabView installed PC to focus the laser on the desired points on the membrane. The microscopic view of the membrane is also fed back to PC and this helps the user to precisely observe and control the position of the focus point.

During optical characterization, 21 points are selected on the diameter of the membrane which are 50 μm apart from each other. The points are given numbers such that the 11^{th} point is the center of the membrane. By obtaining the response of these 21 points to the inputs with frequencies ranging from 3 kHz to 150 kHz, different resonance frequencies with their modal shapes can be obtained. The numbered view of the membrane and the steady-state response of the membrane to the inputs are given in Figure 5.3.

From the data in Figure 5.3 (b), several important properties of the membrane can be obtained. First of all, strong responses are obtained around three frequencies, namely around 28 kHz, 51 kHz and 109 kHz. They are evaluated as the first three resonances of the membrane. The strongest response at each of these frequencies are obtained around the center of the membrane. It is also important that from electrical characterization, it was found that the membrane has 2 resonance frequencies at 1 – 100 kHz frequency band, at 30 kHz and 56 kHz. The first resonance frequency is almost the same in each characterization and this value is similar to the one that is theoretically predicted. The third resonance frequency was not observed during the electrical characterization since the highest frequency of measurement was 100 kHz. Secondly, the modal shapes of each resonance, or mode, are explicit from Figure 5.3 (b). The first mode at 28 kHz, the fundamental mode, has no nulls in its mode shape and strong response at the center. The second mode at 51 kHz has 2 nulls in its mode shape and the third mode at 109 kHz has 4 nulls in its mode shape. It is important that only even mode shapes exist in the membrane which verifies the circular symmetry of it. The modal shapes also verify that the resonance at 28 kHz is the fundamental mode of the membrane. Therefore, it can be concluded that there is no resonance frequency below 28 kHz which is highly important for proper operation of the membrane in the fiber optic MEMS microphone system. In theoretical design of the system, it was discussed that the first resonance frequency being above 20 kHz is important considering the constant phase response.

In the optical measurement setup, OFV5000 laser vibrometer is used together with the displacement decoder of DD-300 which has low frequency cut-off of 30 kHz [38]. In Fig. 5.3, it is observed that the response decays so fast that below 10 kHz, no meaningful response data is observed. The low frequency cut-off of the displacement decoder may be the reason why strong signals at low frequencies could have not been observed. It seems reasonable to state that there is a resonance at 28 kHz and it is the fundamental mode of the membrane due to its modal shape. The response below 28 kHz should be flat, non-decaying shape; however, due to the low frequency cut-off of the displacement decoder DD-300, the response below 28 kHz has a decaying characteristics.

Even the main purpose of the membrane is to sense the audible sound signals, which are in the frequency range of 20 Hz – 20 kHz, it is also highly responsive to the frequencies around 50 kHz and 110 kHz. In some potential further applications that aims to use a membrane operating around 50 kHz or 110 kHz, this design can also be considered.

After analyzing the normalized spatial response of the membrane at different frequencies, the average displacement of the membrane and the displacement of the center point are calculated and plotted as in Figure 5.4 [37].

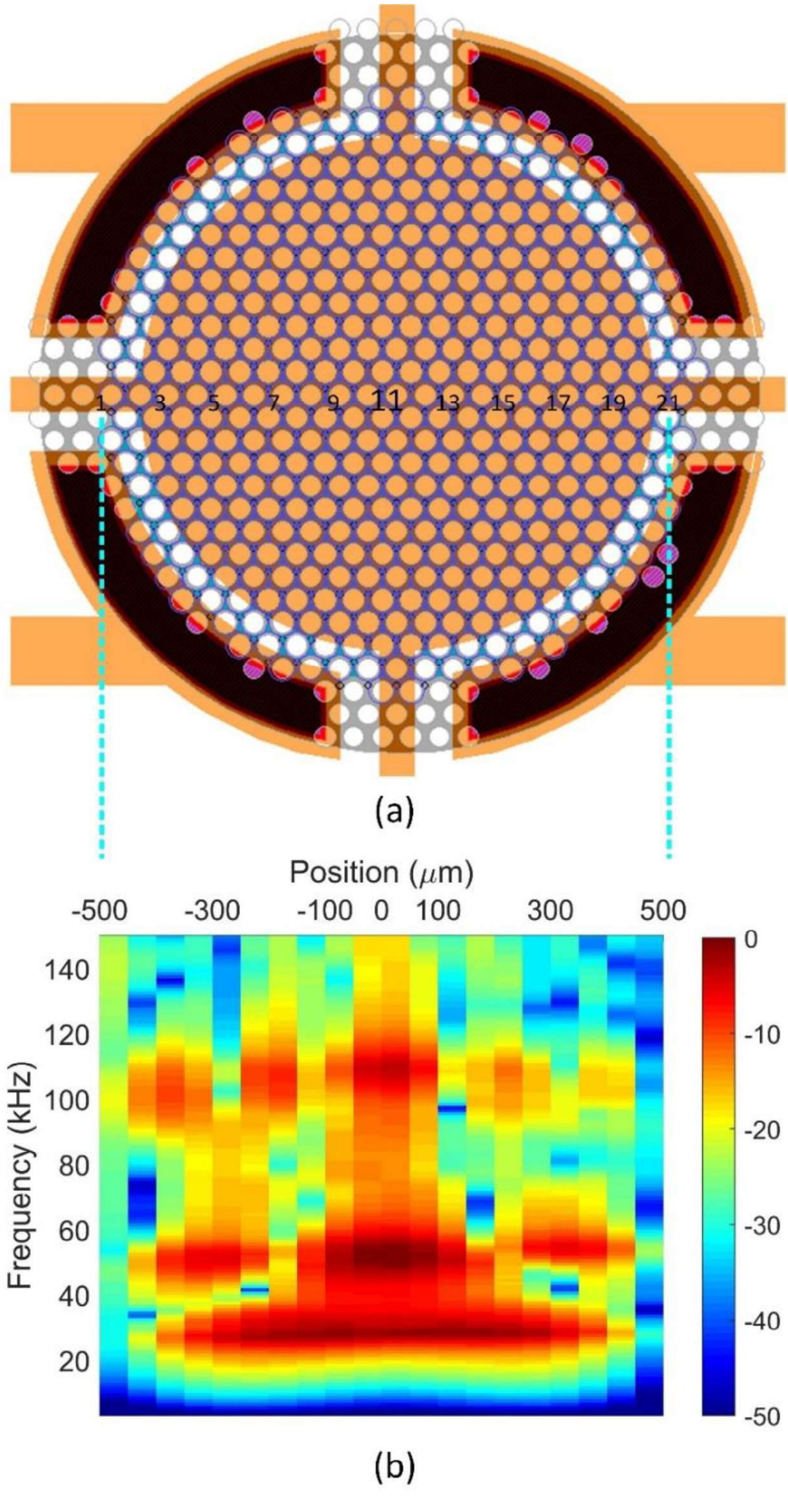

Figure 5.3. (a) The numbered view and (b) steady-state response of the membrane [37].

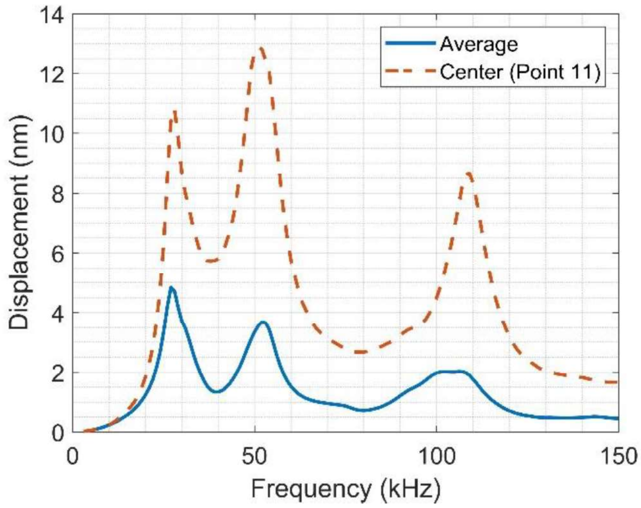

Figure 5.4. Deflection of the membrane as a function of frequency [37].

The displacement of the membrane is 5 nm in average and 10 nm in the center at the first resonance frequency. The quality factor of a resonance can be defined as

$$Q = \frac{f}{f_{BW}} \tag{12}$$

where f is the resonance frequency and f_{BW} is the 3-dB bandwidth of the corresponding resonance. From steady state average deflection data, $f = 28\ kHz$ and $f_{BW} = 6.5\ kHz$ [39]. Therefore, $Q = 4.3$ for the first resonance frequency.

By considering the parallel plate capacitor modal for the membrane, the applied voltage can also be modelled as the force acting on the membrane. In fact, that's why the information obtained from the optical characterization is important; it is required that the membrane is responsive to sound pressure.

The figure of merit to evaluate the performance of the membrane is responsivity. Responsivity of the membrane can be defined as the amount of deflection per unit pressure applied on it. Therefore, in addition to the deflection data, the amount of pressure incident on the membrane should be calculated.

The amount of pressure that acts on the plates of a parallel plate capacitor can be represented as

$$P = \frac{1}{2}\varepsilon E^2 = \frac{1}{2}\varepsilon(\frac{V}{d_{eff}})^2 \tag{13}$$

where $\varepsilon = \varepsilon_0$ which is the permittivity of free space since the material between the plates is air, and the distance between two plates changes on different points on the membrane since at some points there are dimples and at some points there is not. The definition of the effective gap between two plates is required.

For a parallel plate capacitor, deflection of the membrane as s function of the applied voltage can be represented by (14) [40].

$${V_n}^2 = \frac{27}{4} x_n (1 - x_n)^2 \tag{14}$$

V_n can be calculated by (15), where $V_{collapse}$ is the collapse voltage of the membrane [40].

$$V_n = \frac{V}{V_{collapse}} \tag{15}$$

In (14), the other parameter is x_n, where d_{eff} is the effective gap between the plates of the capacitor, can be calculated by (16) [40].

$$x_n = \frac{x}{d_{eff}} \tag{16}$$

From electrical characterization of the membrane, it can be inferred that the collapse voltage, the voltage at which the membrane collapses onto the wafer, is above 3V since when 3V is applied to the membrane, it has still operated properly without any collapse. On the other hand, d_{eff} can be calculated from different regions of the membrane. Namely, let us call the polysilicon regions with dimples as region-1 and polysilicon regions without dimples as region-2. The air gap between the plates of the capacitor in region-1 is $g_1 = 1.25\mu m$ and it is $g_2 = 2\ \mu m$ in region-2. The force acting on each plate can be calculated by (17), where A_1 is the region-1 area and A_2 is the region-2 area.

$$F = \frac{1}{2}\varepsilon\left(\frac{V}{g_1}\right)^2 A_1 + \frac{1}{2}\varepsilon\left(\frac{V}{g_2}\right)^2 A_2 = \frac{1}{2}\varepsilon\left(\frac{V}{d_{eff}}\right)^2 (A_1 + A_2) \tag{17}$$

Here, $\frac{A_1}{A_2} = \frac{1}{9}$ from the design of the membrane. Therefore, it can be concluded that the (18) is valid for the calculation of the effective gap between the plates of the capacitor.

$$\frac{A_1}{A_2}\frac{1}{{g_1}^2} + \frac{1}{{g_2}^2} = (1 + \frac{A_1}{A_2})\frac{1}{{d_{eff}}^2} \tag{18}$$

If the known parameters are put in (18), the effective gap between the plates of the capacitor can be found as $d_{eff} = 1.86\ \mu m$.

If the calculated effective gap is inserted into (14), the collapse voltage is taken as 3 V and the applied voltage is taken as 1 V, which is the actual value in the optical measurement setup, $x_n = 0.01$ is found which indicated that x = 18.6 nm. This value is very small compared to 1.86 µm, so it can be ignored. The meaning of this is that the deflection of the membrane due to the applied DC voltage is negligible compared to the initial effective gap between the plates of the capacitor.

It is important at this point to calculate the responsivity of the membrane. First, the pressure applied on the plates of capacitor should be found. The applied voltage should be studied since it includes both the DC and ac terms. The applied voltage can be written as $V = V_{DC} + v_{ac}\cos(wt)$. The square of the applied voltage is required in pressure calculation. The pressure calculation is as follows for $\varepsilon_0 = 8.854 * 10^{-12}\frac{F}{m}, d_{eff} = 1.86\ \mu m, V_{DC} = 1\ V, v_{ac} = 0.05\cos(wt)\ V$ which are the actual parameters for the membrane and the optical measurement setup.

$$P = \frac{1}{2}\varepsilon E^2 = \frac{1}{2}\varepsilon\left(\frac{V}{d_{eff}}\right)^2 = \frac{1}{2}\varepsilon\left(\frac{V_{DC}+v_{ac}\cos(wt)}{d_{eff}}\right)^2 \tag{19}$$

$$= \frac{1}{2}\frac{\varepsilon}{{d_{eff}}^2}\left(({V_{DC}}^2 + \frac{{v_{ac}}^2}{2}) + 2V_{DC}v_{ac}\cos(wt) + \frac{{v_{ac}}^2}{2}\cos(2wt)\right) \tag{20}$$

If the square of the voltage is considered, there will be three terms: the purely DC term, which is responsible for the change of the effective gap between the plates of the capacitor, the deflection of the membrane, one purely ac term with angular frequency of w, and another purely ac term with angular frequency of $2w$. The ac term with angular frequency of $2w$ should not be considered in pressure calculation since this response is not at the same frequency with the input. The only term that should be considered in this calculation is the ac term with angular frequency of w since it is the only responsible term for the deflection of the membrane due to the input with angular frequency of w.

$$P \cong \frac{1}{2}\frac{\varepsilon}{{d_{eff}}^2}(2V_{DC}v_{ac}\cos(wt)) \tag{21}$$

$$= \frac{8.854*10^{-12}}{2*(1.86*10^{-6})^2}(2*1*0.05) = 0.128\ Pa \tag{22}$$

From the average displacement data obtained from the optical measurement setup, it is known that the average displacement of the membrane at 28 kHz is 5nm. During the pressure calculation, the reason that the peak pressure is used is that the output of the vibrometer is also the peak value, so the division of the displacement with pressure is proper. Therefore, the responsivity at the first resonance frequency, at 28 kHz, can be calculated from as 39 nm/Pa [37].

$$Responsivity = \frac{\Delta d_{membrane}}{P} = \frac{5\ nm}{0.128\ Pa} = 39\ nm/Pa \tag{23}$$

It is predicted that with the increasing applied DC bias, the average displacement will increase. Hence, by operating the membrane at a DC bias of 3V, higher response can be obtained from the membrane which results tin easier detection of the displacement by the laser light in fiber optic MEMS microphone application.

Since the membrane will be used in the fiber optic MEMS microphone application, a laser light will be directed to the membrane. The area that the laser light to be spotted is highly critical since the width of the beam increases with distance. In other words, first the light will be sent to the membrane and then it will hit back from the metal coated, reflective surface of the membrane. During this travel, the width of the light will increase and only the limited amount of the reflected light will be sensed due to the fixed diameter of the fiber. To obtain the greatest amount of the reflected light with the optimum deflection information, the area that the light will be focused should be studied. As the amount of the light that is coupled decreases, the power of the light decreases which decreases the signal level that is obtained from the photodetector. As a result, the signal to noise (SNR) of the measurement will decrease.

Since the first resonance frequency, 28 kHz, is critical for the operation of the membrane in the fiber optic MEMS microphone system, this analysis will be done only for this frequency. To decide where to focus the laser light to obtain the maximum deflection information per area, the responses of the data points are used. Circular shaped areas are considered since the laser light spot will be in circular shape. Average displacement over the selected area is obtained for different radial distances from the center of the membrane. The resultant characteristics is shown in Figure 5.5 [37].

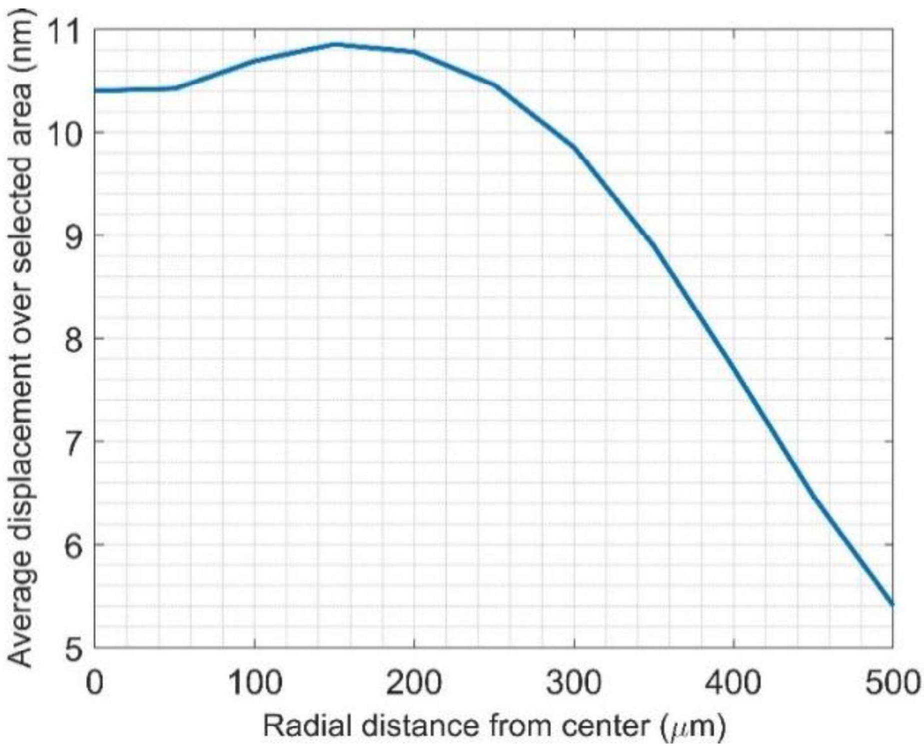

Figure 5.5. Average displacement over the selected area for different radial distances [37].

The radius of the optimum area to focus the light is 150 µm. Besides, it is observed that the average displacement per the selected area remains almost constant for the areas with radius 50 – 250 µm. Therefore, it will be optimum to focus the laser light to the 300 µm – diameter circular area. This selection will optimize both the sensitivity of the measurement and the amount of light that couples back to the fiber.

The symmetry of the membrane is important for proper operation and for the verification of the microfabrication process on reliability and reproducibility. Even some information is extracted from the steady-state response spatial data given in Figure 5.3 (b). To investigate the symmetry of the membrane further, the data from the points that are 50 µm, 150 µm, 250 µm and 350 µm distant from the center of the membrane is used. The obtained characteristics is as in Figure 5.6 [37].

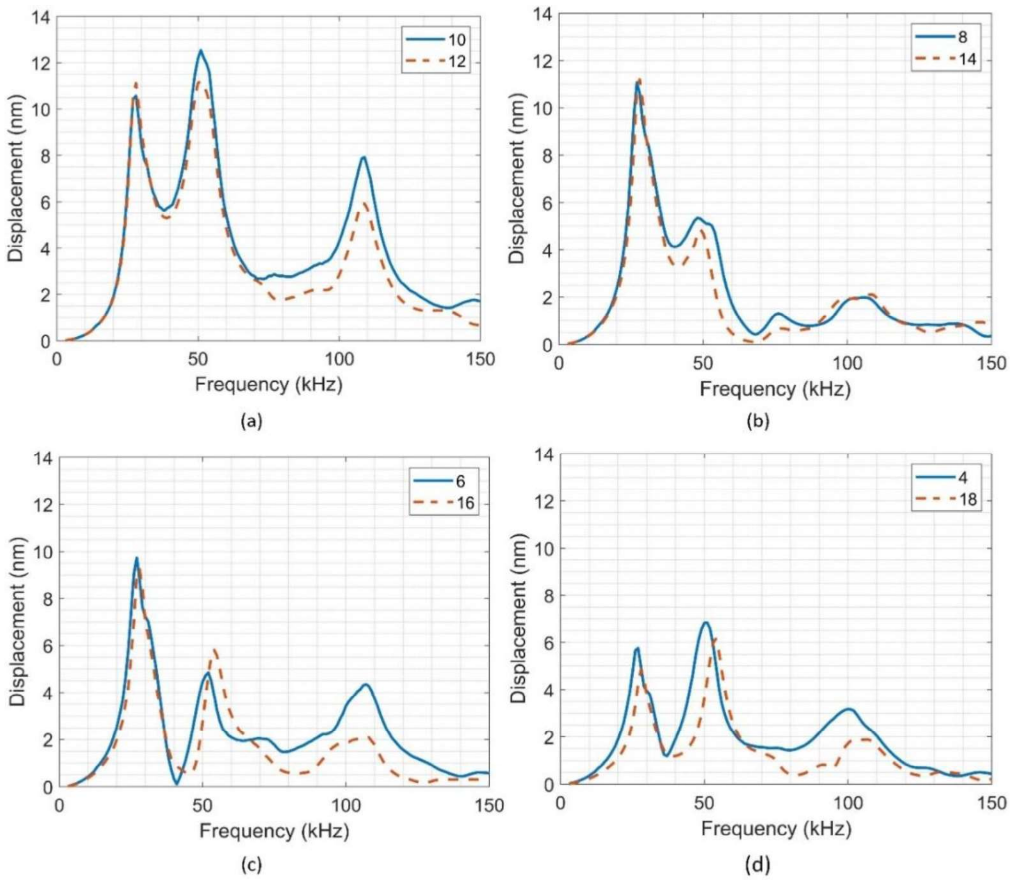

Figure 5.6. Response of wo points that are (a) 50 µm, (b) 150 µm, (c) 250 µm and (d) 350 µm distant from the center of the membrane [37].

In Figure 5.6 (a), it is observed that the peak responses of the points that are 50 µm distant from the center of the membrane are at the same frequencies. This symmetry can also be observed in Figure 5.6 (b) for the points that are 150 µm distant from the center of the membrane. For the points that are 250 µm distant from the center of the membrane, in Figure 5.6 (c), the location of the second resonance frequency changes slightly by 3.8 %. In Figure 5.6 (d), further small deviations are observed for the points that are 350 µm distant from the center of the membrane: the first, second and third resonance frequencies change by 3.6 %, 5.9 % and 4 %, respectively. It can be concluded from the data in Figure 5.6 (a),(b),(c) that the membrane is highly symmetric in the circular area with radius of 250 µm [37].

The temporal transient response is another important characteristics of the membrane. To obtain the temporal transient response of the membrane, single cycle sinusoidal signals at 28 kHz, 51 kHz and 109 kHz are used. The spatial steady state responses of the membrane to the input signals at 28 kHz, 51 kHz and 109 kHz are given in Figure 5.7 (a). The temporal transient responses are given in Figure 5.7 (b),(c),(d) at frequencies of 28 kHz, 51 kHz and 109 kHz, respectively [37].

The symmetry of the membrane can also be observed from Figure 5.7 (a). The steady-state response of the membrane to the sinusoidal inputs at the resonance frequencies verify the circular symmetry of the membrane. In Figure 5.7 (b), (c), (d), the transient ringing responses are observed and the transient response of the membrane to the input at 28 kHz has the longest ringing response. All of the transient responses decay with time. Since the transient response is obtained for 21 points on the main diameter of the membrane, the symmetry can also be observed from temporal transient response.

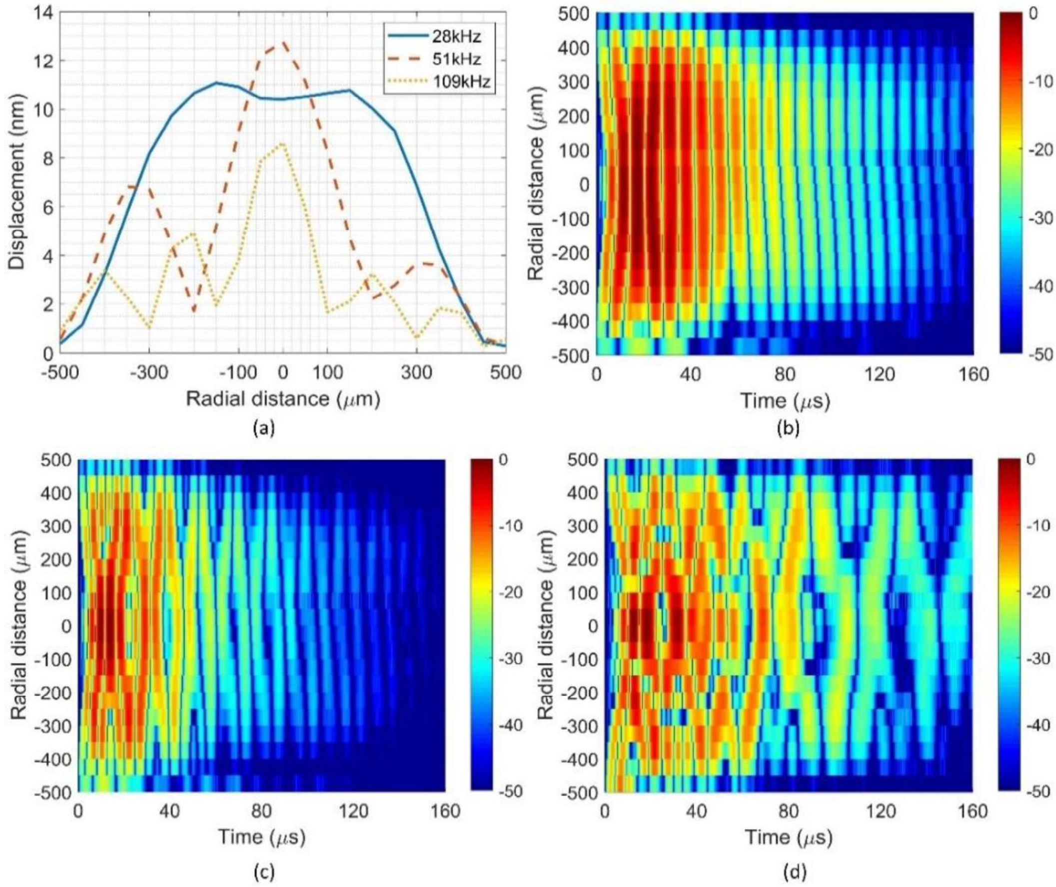

Figure 5.7. Spatial response of the membrane to the (a) CW inputs at 28 kHz, 51 kHz and 109 kHz (steady-state response), and single cycle of sine pulses at (b) 28 kHz, (c) 51 kHz, (d) 109 kHz (transient response) [37].

The quality factor of a resonance can also be calculated from its transient response and it is given as

$$Q = \pi * \frac{\tau}{T} \tag{24}$$

where T is the period of excitation (35.7 μs for the fundamental mode) and τ is the time constant of the decay which is found as 46 μs for the fundamental mode. Therefore, the quality factor of the first resonance is calculated as $Q = 4$ from transient analysis.

CHAPTER 6

CONCLUSION

The membrane of a fiber optic MEMS microphone is designed and microfabricated. The design is based on the theoretical analysis of a membrane which suggests the dimensions of a membrane to achieve high sensitivity in the audible frequency range. In addition to the dimension decision, the microfabrication process is selected according to the experiences in the literature and the needs of the current design.

The designed membrane featuring 1000 μm-diameter, 1.5 μm-thick is microfabricated by POLYMUMPS process and it has 36 μm-diameter air holes. The air holes are used such that the sacrificial oxide etch is achieved without any problem. The dimensions and the arrangement of the holes are designed to obtain the fill factor of 53 %. The surface of the designed membrane is coated with gold which is an optically reflective surface since the membrane is to be used in a fiber optic MEMS microphone.

The characteristics of the design is investigated through electrical and optical measurements via impedance analyzer and laser vibrometer, respectively. The resonance frequencies and modal shapes in each frequency is obtained by advanced analysis of the results obtained from these measurements. The first resonance of the membrane, the fundamental mode frequency, changes by 3 % when the applied DC bias voltage changes from 0 V to 3 V. The higher order modes and their modal shapes are also obtained from the spatial frequency response data and the center of the membrane gives strong response to the inputs at its resonance frequencies.

The modal shapes suggest that the membrane is highly symmetric and the modal shape of the resonance at 28 kHz indicates that it is the first resonance frequency. The strong response and almost no phase reversal in the audible frequency range is obtained by utilizing the first resonance frequency above the audible frequency range, at 28 kHz.

The membrane design is suitable for the fiber optic MEMS microphone application due to its high sensitivity, 40 nm/Pa, and high circular symmetry which is highly important due to the circular spots of the laser light. It is also possible to select the area to focus the light on the membrane since the response is almost the same within the 250 μm-radius area. This flexibility is valuable for fiber optic MEMS microphone application since the optical unit of the system may require different focusing areas. The characteristics of the membrane design are investigated from different perspectives and the design is verified to be suitable for fiber optic MEMS microphones.

As a future work, the wafer can be grinded from the bottom such that the substrate thickness decreases. By this way, absorption of the laser light can be decreased which may increase the quality of optical detection. The reliability of the membrane can also be tested via long term (>1 hour) usage.

REFERENCES

[1] Manish Kumar Mishra, Vikas Dubey, P. M. Mishra, Isharat Khan, "MEMS Technology: A Review", Journal of Engineering Research and Reports, 4(1): 1-24 (2019).

[2] Byung-Hun Kim, Hwa-Sun Lee, "Acoustical-Thermal Noise in a Capacitive MEMS Microphone", IEEE Sensors Journal, Vol. 15, No. 12 (2015).

[3] S. Walser, C. Siegel, M. Winter, G. Feiertag, M. Loibl, A. Leidl, "MEMS microphones with narrow sensitivity distribution", Sensors and Actuators, A247 663-670 (2016).

[4] Chonghua Zhou, Stephen V. Letcher, and Arun Shukla, "Fiber-optic microphone based on a combination of Fabry–Perot interferometry and intensity modulation", The J. Acoust. Soc. Am., 98, 1042 (1995).

[5] Ming Li, Ming Wang,"Optical MEMS pressure sensor based on Fabry-Perot interferometry", Optics Express, Vol. 14, No.4 (2006).

[6] Ji-Huan Chen, Xu-Guang Huang, Jia-Rong Zhao, Jin Tao, Wei-Xin He, Song-Hao Liu, "Fabry–Perot interference-based fiber-optic sensor for small displacement measurement", Optics Communications 283, 3315–3319 (2010).

[7] J. A. Bucaro, H. D. Dardy, and E. F. Carome, "Fiber-optic hydrophone", J. Acoust. Soc. Am., 62, 1302 (1998).

[8] Qingxu YU and Xinlei ZHOU, "Pressure Sensor Based on the Fiber-Optic Extrinsic Fabry-Perot Interferometer",Photonic Sensors Vol. 1, No. 1: 72-83 (2011).

[9] Zhenfeng Gong, Ke Chen, Xinlei Zhou, Yang Yang, Zhihao Zhao, Helin Zou, and Qingxu Yu, "High Sensitivity Fabry-Perot Interferometric Acoustic Sensor for Low-Frequency Acoutic Pressure Detections", J. Lightwave Tech., Vol. 35, No. 24 (2017).

[10] Yu Wu, Caibin Yu, Fan Wu, Chen Li, Jinhao Zhou, Yuan Gong, Yunjiang Rao, Yuanfu Chen, "A Highly Sensitive Fiber-Optic Microphone Based on Graphene Oxide Membrane", J. Lightwave Tech., Vol. 35, No. 19 (2017).

[11] Bin Liu, Han Zhou, Lei Liu, Xing Wang, Mingguang Shan, Peng Jin, Zhi Zhong, "An Optical Fiber Fabry-Perot Microphone Based on Corrugated Silver Diaphragm", IEEE Transactions on Instrumentation and Measurement, Vol. 67, No. 8 (2018).

[12] Xueqi Lu, Yu Wu, Yuan Gong, Yunjiang Rao, "A miniature fiber-optic microphone based on annular corrugated MEMS diaphragm", J. Lightwave Tech., doi: 10.1109/JLT.2018.2868964 (2018).

[13] “POLYMUMPS Design Rules” retrieved from “http://www.memscap.com/products/mumps/polymumps/reference-material”, on 1st of November 2017.

[14] S. Fouladi, M. Bakri-Kassem, R.R. Mansour, “Suspended on-chip RF MEMS components fabricated using PolyMUMPs technology”, Can. J. Elect. Comput. Eng., Vol. 31, No. 2 (2016).

[15] Tanom Lomas, Adisorn Tuantranont, Anurat Wisitsoraat, “Polysilicon Piezoresistive Tactile Sensor Array Fabricated by PolyMUMPs Process”, IEEE Sensors (2006).

[16] Sae-Won Lee, Robert Johnstone, Ash M. Parameswaran, “MEMS Mechanical Logic Units: Design and Microfabrication with Micragem and POLYMUMPS”, IEEE CCECE/CCGEI (2005).

[17] Wei Wu, David W. Greve, Irving J. Oppenheim, “Characterization and Noise Analysis of Capacitive MEMS Acoustic Emission Transducers”, IEEE Sensors (2007).

[18] Adisorn Tuantranont, Tanom Lomas, Kata Jaruwongrungsee, Apichai Jomphoak, Anurat Wisitsoraat, “Symmetrical PolyMUMPs-Based Piezoresistive Microcantilever Sensors with On-Chip Temperature Compensation for Microfluidics Applications”, IEEE Sensors Journal, Vol. 8 No. 5 (2008).

[19] “Xin Guo, Kongying Xie, Raobert J. Campbell, Yongjun Lai, “A study on three-dimensional electrode arrays fabricated by PolyMUMPs for AC electro-osmotic pumping”, Microelectronic Engineering, Vol. 88, Issue 10 (2011).

[20] Sheplak, M., Breuer, K.S., Schmidt, M.A. “A wafer-bonded, silicon nitride membrane microphone with dielectrically-isolated single crystal silicon piezoresistors”, Proc. Solid-State Sens. Actuator Workshop, Hilton Head Island, SC, 23–26 (1998).

[21] Sheplak, M., Seiner, M., Breuer, K.S., Schmidt, M.A. “A MEMS microphone for aeroacoustic measurements”, 37th AIAA (1999).

[22] Huang, C., Naguib, A., Soupos, E., Najafi, K. “A silicon micromachined microphone for fluid mechanics research”. J. Micromecha. Microeng., 12(6), 767–774 (2002).

[23] Scheeper, P.R., Nordstrand,B., Gullov, B.L.J.O., Clausen, T., Midjord, L., Storgaard-Larsen, T. ” A new measurement microphone based on MEMS technology”, J. Microelectromech. Syst., 12(6),880–891 (2003).

[24] Martin,D.T., Kadirvel, K., Liu, J.,Fox, R.M., Sheplak, M., Nishida, T., “Surface and bulk micromachined dual back-plate condenser microphone”, Proc. 18th IEEE Int. Conf. MEMS, Miami, FL,319–322 (2005).

[25] Martin, D.T., Jian, L., Kadirvel, K., Fox, R.M., Sheplak, M., Nishida, T., "A micromachined dual-backplate capacitive microphone for aeroacoustic measurements", Journal of Microelectromechanical Systems, Vol. 16, Issue 6 (2007).

[26] Martin, D.T., Kadirvel, K., Nishida, T., Sheplak,M., "A surface micromachined capacitive microphone for aeroacoustic applications", Proc. Solid-State Sens., Actuator, Microsyst. Workshop, Hilton Head, SC, 1–4 (2008).

[27] Chan, C. K., Lai, W. C., Wu, M., Fang, W., "Design and implementation of a novel double-poly microphone with rigid acoustic receiver, flexible spring supporter, and harm backplate", Micro Electro Mechanical Systems (MEMS), 2010 IEEE 23rd International Conference, 651-654 (2010).

[28] Yang, C. T., "The sensitivity analysis of a MEMS microphone with different membrane diameters.", Journal of Marine Science and Technology,18(6), 790-796 (2010).

[29] Chao, P. C. P., Tsai, C. Y., Chiu, C. W., Tsai, C. H., Tu, T. Y., "A new hybrid fabrication process for a high sensitivity MEMS microphone", Microsystem technologies, 19(9-10), 1425-1431 (2013).

[30] Franz, J., "Piezoelektrische sensoren auf siliziumbasis für akustische anwendungen," Ph.D. Thesis, Darmstadt Technology University, Darmstadt, Germany(1988)

[31] Horowitz, S.,Nishida, T., Cattafesta, L.,Sheplak, M. "Development of a micromachined piezoelectric microphone for aeroacoustics Applications". J. Acoust. Soc. Amer. 122(6), 3428–3436 (2007).

[32] Littrell, R.J., "High performance piezoelectric MEMS microphones," Ph.D. Thesis, Univ. Michigan, Ann Arbor, MI. (2010)

[33] Grosh, K., Littrell,R., "Piezoelectric MEMS Microphone "Patent Number: US 8,531,088 (2013).

[34] Lee, W. S., Lee, S. S. "Piezoelectric microphone built on circular diaphragm". Sensors and Actuators A: Physical, 144(2), 367-373 (2008).

[35] Retrieved from "https://www.cdc.gov/ncbddd/hearingloss/sound.html", on 26th of October, 2017.

[36] Keysight E5061B ENA Vector Network Analyzer Data Sheet

[37] Goktug Cihan Ozmen, Ilker Oguz, Asaf Behzat Sahin, Baris Bayram, "Design and Characterization of a MEMS Membrane for a Fiber Optic Microphone", Journal of Acoustical Society of America, Manuscript Number JASA-04307 (under review).

[38] Datasheet for DD-300 24 MHz Displacement Decoder specifications.

[39] Park, Kwan Kyu, Lee, Hyunjoo, Crisman, P, Kupnik, Mario, Oralkan, O, Khuri-Yakub, Pierre, “Optimum design of circular CMUT membranes for high quality factor in air” 504 - 507. 10.1109/ULTSYM.2008.0123 (2008).

[40] G. G. Yaralioglu, A. S. Ergun, B. Bayram, E. Haeggstrom and B. T. Khuri-Yakub, "Calculation and measurement of electromechanical coupling coefficient of capacitive micromachined ultrasonic transducers,", *IEEE Transactions on Ultrasonics, Ferroelectrics, and Frequency Control*, vol. 50, no. 4, pp. 449-456, (2003).